Please cite this article in press as: Tuzon et al., Concerted Activities of Distinct H4K20 Methyltransferases at DNA Double-Strand Breaks Regulate 53BP1 Nucleation and NHEJ-Directed Repair, Cell Reports (2014), http://dx.doi.org/10.1016/j.celrep.2014.06.013

Cell Reports
Report

Concerted Activities of Distinct H4K20 Methyltransferases at DNA Double-Strand Breaks Regulate 53BP1 Nucleation and NHEJ-Directed Repair

Creighton T. Tuzon,[1] Tanya Spektor,[1] Xiaodong Kong,[2] Lauren M. Congdon,[1] Shumin Wu,[1] Gunnar Schotta,[3] Kyoko Yokomori,[2] and Judd C. Rice[1,*]
[1]Department of Biochemistry and Molecular Biology, Norris Comprehensive Cancer Center, Keck School of Medicine, University of Southern California, Los Angeles, CA 90033, USA
[2]Department of Biological Chemistry, School of Medicine, University of California at Irvine, Irvine, CA 92697, USA
[3]Munich Center for Integrated Protein Science, Adolf-Butenandt-Institute, Ludwig Maximilian University, Munich 80336, Germany
*Correspondence: juddrice@usc.edu
http://dx.doi.org/10.1016/j.celrep.2014.06.013

SUMMARY

Although selective binding of 53BP1 to dimethylated histone H4 lysine 20 (H4K20me2) at DNA double-strand breaks (DSBs) is a necessary and pivotal determinant of nonhomologous end joining (NHEJ)-directed repair, the enzymes that generate H4K20me2 at DSBs were unclear. Here, we determined that the PR-Set7 monomethyltransferase (H4K20me1) regulates de novo H4K20 methylation at DSBs. Rapid recruitment of PR-Set7 to DSBs was dependent on the NHEJ Ku70 protein and necessary for NHEJ-directed repair. PR-Set7 monomethyltransferase activity was required, but insufficient, for H4K20me2 and 53BP1 nucleation at DSBs. We determined that PR-Set7-mediated H4K20me1 facilitates Suv4-20 methyltransferase recruitment and catalysis to generate H4K20me2 necessary for 53BP1 binding. The orchestrated and concerted activities of PR-Set7 and Suv4-20 were required for proficient 53BP1 nucleation and DSB repair. This report identifies PR-Set7 as an essential component of NHEJ and implicates PR-Set7 as a central determinant of NHEJ-directed repair early in mammalian DSB repair pathway choice.

INTRODUCTION

p53-binding protein 1 (53BP1) is a critical component in mammalian DNA damage response (DDR), and recruitment of 53BP1 to double-strand breaks (DSBs) is a necessary and pivotal determinant of nonhomologous end joining (NHEJ)-directed repair (Panier and Boulton, 2014). Increasing evidence indicates that 53BP1 recruitment to chromatin near DSBs is dependent on proficient binding of the 53BP1 tandem Tudor domains to dimethylated histone H4 lysine 20 (H4K20me2), which is required for competent 53BP1 nucleation at DSBs, mass accumulation of 53BP1 at irradiation-induced foci (IRIF), immunoglobulin class switch recombination (CSR), and NHEJ-directed repair (Bothmer et al., 2011; Botuyan et al., 2006; Bunting et al., 2010; Sanders et al., 2004). Consistent with this, recent reports demonstrate that 53BP1 binding to H4K20me2 is obstructed by acetylation of neighboring H4K16 and, conversely, H4K16 deacetylation robustly augments 53BP1-H4K20me2 binding, resulting in enhanced 53BP1 nucleation at DSBs and 53BP1 IRIF (Hsiao and Mizzen, 2013; Tang et al., 2013). 53BP1 chromatin interaction is further strengthened by additional histone modification, including ubiquitinated H2AK15 that binds the 53BP1 ubiquitination-dependent recruitment domain but only in an H4K20me2-dependent manner (Fradet-Turcotte et al., 2013). Whereas these findings indicate that H4K20me2 is an essential determinant of 53BP1 chromatin binding and NHEJ-directed repair, the upstream enzymatic mechanisms that facilitate H4K20me2 at DSBs were undetermined.

Because H4K20me2 is highly abundant, accounting for >80% of total H4 in human cells, the necessity for de novo H4K20me2 at DSBs was unclear (Pesavento et al., 2008). Due to the abundance of H4K20me2, it was postulated that the likely presence of preexisting H4K20me2 near DSBs may suffice for 53BP1 binding; however, rigorous examination of this model is currently lacking (Sanders et al., 2004). A recent report seemed to support the model demonstrating that H4K20me2 near a DSB was only slightly elevated immediately after induction of the DSB, but 53BP1 occupancy increased ~2-fold (Hsiao and Mizzen, 2013). At later time points following DSB induction, however, H4K20me2 and 53BP1 near the DSB were reported to be significantly elevated (~20-fold; Pei et al., 2011). These results indicated that de novo H4K20me2 occurs at DSBs, but the H4K20 methyltransferases responsible and their biological significance in DSB repair were unclear.

In this report, we determined that the orchestrated and concerted activities of the PR-Set7 H4K20 monomethyltransferase (H4K20me1) and Suv4-20 dimethyltransferases (H4K20me2) are required for de novo H4K20me2 near DSBs (Nishioka et al., 2002; Schotta et al., 2004). We found that the reported rapid recruitment of PR-Set7 to DSBs is dependent on the NHEJ Ku70 protein, which interacts with PR-Set7 in cells (Oda et al.,

Please cite this article in press as: Tuzon et al., Concerted Activities of Distinct H4K20 Methyltransferases at DNA Double-Strand Breaks Regulate 53BP1 Nucleation and NHEJ-Directed Repair, Cell Reports (2014), http://dx.doi.org/10.1016/j.celrep.2014.06.013

2010). Consistent with a role in NHEJ-directed repair, depletion of PR-Set7 and H4K20me1 severely impaired 53BP1 recruitment and NHEJ repair activity. Although 53BP1 was reported to bind H4K20me1 in vitro, we found that PR-Set7-mediated H4K20me1 is insufficient for 53BP1 nucleation in cells (Botuyan et al., 2006; Oda et al., 2010). We determined that PR-Set7-mediated H4K20me1 functions to facilitate de novo H4K20me2 by promoting Suv4-20 recruitment and catalysis, consistent with reports demonstrating that H4K20me1 is the preferred substrate for Suv4-20 catalysis (Schotta et al., 2008; Southall et al., 2014; Wu et al., 2013). Suv4-20-mediated H4K20me2 was necessary for 53BP1 nucleation near DSBs, consistent with reports demonstrating that Suv4-20 depletion impairs 53BP1 IRIF (Hsiao and Mizzen, 2013; Yang et al., 2008). This study reveals a progressive PR-Set7-dependent pathway required for proficient de novo H4K20me2 at DSBs, 53BP1 nucleation, and DSB repair. Furthermore, this study identifies PR-Set7 as an essential factor of NHEJ that likely promotes NHEJ-directed repair early during mammalian DSB repair pathway selection.

RESULTS

Rapid and Focal Recruitment of PR-Set7 to DSBs Is Necessary for Proficient DSB Repair

Prolonged PR-Set7 depletion results in the expected ablation of H4K20me1 but also reduced H4K20me2, coincident with phenotypes indicative of defective DSB repair, including elevated and sustained activation of canonical DDR proteins and unrepaired DSBs (Hartlerode et al., 2012; Houston et al., 2008; Oda et al., 2009). To exclude the possibility that defective DSB repair was an indirect consequence of reduced H4K20me2, U2OS cells were transduced with a control small hairpin RNA (shRNA) or shRNA targeting the 3′ UTR of endogenous *PR-Set7* for 4 days to deplete PR-Set7 and reduce global H4K20me1, but not H4K20me2, prior to treatment with sublethal doses of ionizing radiation (IR) (Figures S1A and S1B). Short-term PR-Set7 depletion resulted in the rapid and significant decline of viable U2OS cells following low-level IR exposure compared to control cells (Figure 1A). Because the nonirradiated PR-Set7 shRNA U2OS cells displayed no measurable changes in cell viability compared to control, the enhanced radiosensitivity of cells following short-term PR-Set7 depletion was not due to proliferative or cell cycle perturbations observed following prolonged PR-Set7 depletion.

Whereas these results demonstrate that PR-Set7 is necessary for proficient DSB repair, it remained unclear whether PR-Set7 functions in DDR and/or directly in DSB repair. To assess the role of PR-Set7 in DDR checkpoint activation, early passage diploid human foreskin fibroblasts (HFFs) transduced with control or PR-Set7 shRNA were subjected to increasing doses of IR (Figure 1B). Western blot analysis revealed that the dose-dependent activation of the canonical DDR checkpoint proteins, ATM, ATR, p53, and H2A.X, were nearly identical between control and PR-Set7-depleted cells, indicating that PR-Set7 is dispensable for the initial activation of these DDR proteins. Conversely, a potential direct role for PR-Set7 in DSB repair was inferred following low-energy laser irradiation of GFP-PR-Set7-expressing HeLa cells (Kong et al., 2009). Fluorescence microscopy revealed that GFP-PR-Set7 rapidly mobilized and remained at laser-induced DSBs for >30 min in contrast to GFP-null control, consistent with a previous report (Figures S1C and S1D) (Oda et al., 2010).

These cytological observations suggested that PR-Set7 is directly recruited to DSBs. To test this hypothesis at a defined DSB in cells, murine embryonic stem cells (mESCs) containing an integrated *DR-GFP* transgene were electroporated with an *I-SceI* expression plasmid to create a genome-specific induced DSB (iDSB) prior to chromatin immunoprecipitations (ChIPs) and quantitative PCR (qPCR) (Figure 1C) (Donoho et al., 1998). ChIP-qPCR analysis confirmed the iDSB by significant H2A.X phosphorylation (γH2A.X) throughout the transgene compared to the negative control *GAPDH* (Figures 1D and S1E). Significant enrichments of PR-Set7 and methylated H4K20 relative to H3 control were observed near the iDSB (−1 kb and −2 kb), but none were detected more distal to the iDSB at +5 kb (Figures 1D, S1F, and S1G). Identical results were obtained in U2OS *DR-GFP* cells (Figure S1H). The NHEJ Ku70 protein displayed similar enrichment patterns, indicating that PR-Set7 recruitment and de novo H4K20 methylation are focally localized to a region near the iDSB.

U2OS cells containing different integrated *I-SceI* reporter transgenes were utilized to delineate the role of PR-Set7 in NHEJ (EJ5-GFP), single-strand annealing (SSA-GFP), and homology-directed repair (HDR-GFP) (Gunn and Stark, 2012). Following induction of the DSB in control and PR-Set7-depleted cells, proficient iDSB repair was assessed by flow cytometry of GFP+ cells. Compared to control, PR-Set7 depletion significantly reduced iDSB repair by NHEJ and significantly increased repair by SSA and HDR (Figure 1E). These findings indicate that PR-Set7 recruitment to DSBs is necessary for NHEJ-directed repair.

De Novo H4K20 Methylation and 53BP1 Nucleation Are Dependent on PR-Set7 Monomethyltransferase Activity

PR-Set7 may function in repair pathway choice by facilitating H4K20me2 near DSBs necessary for binding of 53BP1, a pivotal determinant of NHEJ-directed repair (Panier and Boulton, 2014). Consistent with this, several reports demonstrated that prolonged PR-Set7 depletion reduced global H4K20me2 levels and impaired 53BP1 IRIF (Botuyan et al., 2006; Hartlerode et al., 2012; Oda et al., 2010). Although short-term PR-Set7-depleted HeLa cells retained wild-type H4K20me2 levels, we unexpectedly observed impaired 53BP1 IRIF (Figures 2A and S1B). To determine whether this defect was due to loss of PR-Set7 catalytic activity, HeLa cells were transfected with a dominant negative PR-Set7 catalytically dead (CD) point mutant (Sims and Rice, 2008). These cells also displayed impaired 53BP1 IRIF, consistent with previous reports, indicating that PR-Set7 monomethyltransferase activity, but not PR-Set7 per se, is required for proficient 53BP1 IRIF (Figure 2A) (Hartlerode et al., 2012; Houston et al., 2008; Oda et al., 2010).

The results suggested that PR-Set7 recruitment is necessary for de novo H4K20 methylation and 53BP1 nucleation near DSBs. To test this, U2OS *DR-GFP* cells were transduced with a control or PR-Set7 shRNA to deplete PR-Set7 prior to *I-SceI* transfection (Bennardo et al., 2009). ChIP-qPCR demonstrated that PR-Set7 depletion did not affect γH2A.X enrichment but resulted in the ablation of H4K20me1 and significant reductions

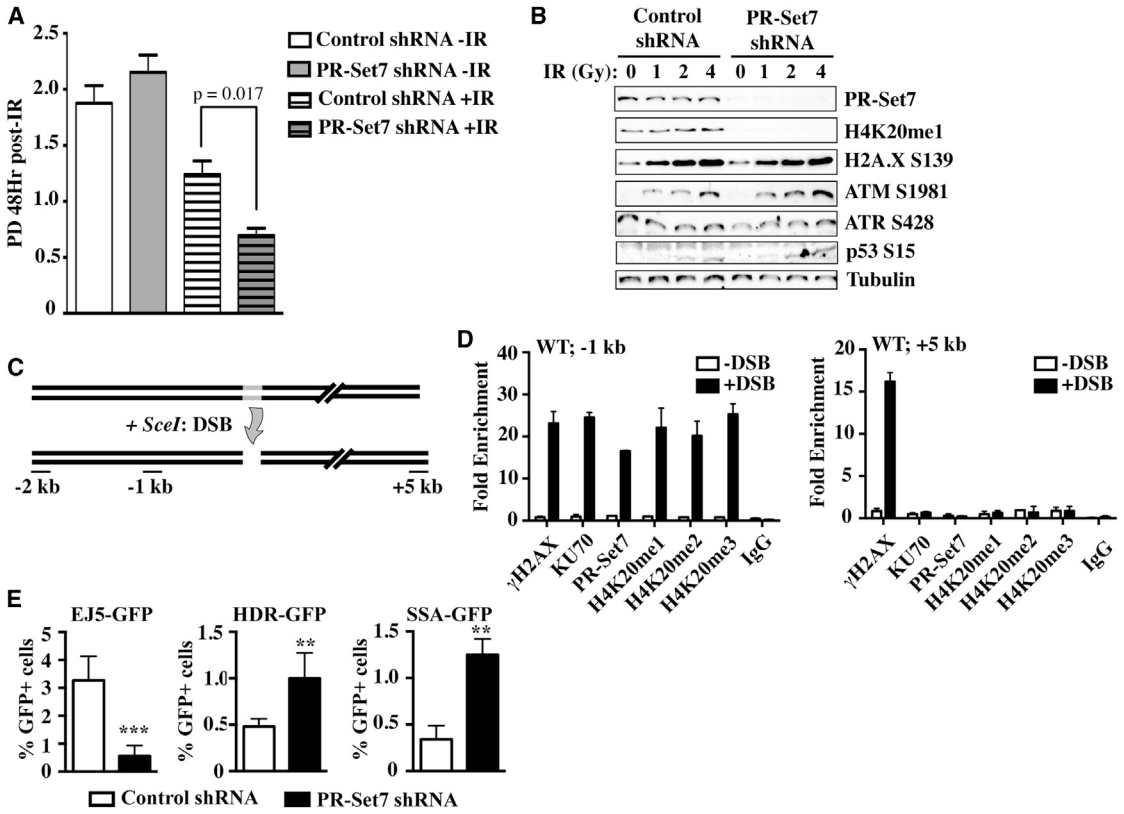

Figure 1. Recruitment of PR-Set7 to DSBs Is Necessary for NHEJ-Directed Repair

(A) U2OS cells transduced with control or PR-Set7 shRNA were irradiated (2 Gy) 48 hr posttransduction. Population doublings (PD) were calculated by monitoring cell viability by trypan blue exclusion 48 hr following IR (*y* axis). Values represent the mean ± SD from five independent biological replicates. The Student's t test was used to determine statistical significance as indicated.

(B) Early passage human foreskin fibroblast cells transduced with control or PR-Set7 shRNA were irradiated with the indicated doses. Whole-cell lysates were collected 1 hr postirradiation for western blot analysis using the indicated antibodies.

(C) Illustration of the *DR-GFP* transgene and locations of the qPCR amplicons.

(D) ChIP-qPCR analysis of wild-type (WT) *DR-GFP* mESCs in the absence (−DSB) or presence (+DSB) of *I-SceI* using the indicated antibodies (*x* axis) and qPCR amplicons. Values represent the mean fold enrichment relative to histone H3 ± SD from five independent biological replicates. IgG, immunoglobulin.

(E) Control or PR-Set7 shRNA U2OS cells containing integrated *I-SceI*-GFP reporters were used to measure NHEJ (EJ5-GFP), single-strand annealing (SSA-GFP), and HDR (HDR-GFP) activity by flow cytometry. Values represent the mean GFP+ cells ± SD from six independent biological replicates. The Student's t test was used to determine statistical significance between control and PR-Set7 shRNA as indicated: $p < 0.0001$ (***), $p = 0.0012$ (**), $p = 0.0024$ (**). See also Figure S1.

in H4K20me2, H4K20me3, and 53BP1 occupancy near the iDSB compared to control, as hypothesized (Figures 2B and S2A). Complementation experiments were performed in PR-Set7-depleted U2OS *DR-GFP* cells transfected with either wild-type FLAG-PR-Set7 (WT) or -PR-Set7 CD (Figure S2B). ChIP-qPCR analysis demonstrated that, whereas recruitment of PR-Set7 WT restored de novo H4K20 methylations near the iDSB, recruitment of PR-Set7 CD did not (Figures 2C, 2D, S2C, and S2D). To determine whether PR-Set7 recruitment is sufficient for de novo H4K20 methylations and 53BP1 nucleation at loci regardless of DNA damage, human embryonic kidney 293 (HEK293)-TK22 cells containing an integrated *5xGAL4-UAS-TK-Luc* reporter transgene were transfected with a GAL4-DBD-control, -PR-Set7 WT, or -PR-Set7 CD plasmid (Figure S3A) (Ishizuka and Lazar, 2003). ChIP-qPCR analysis demonstrated that specific localization of PR-Set7 WT to the undamaged transgene resulted in significantly increased H4K20 methylations and 53BP1 occupancy (Figures 3A and S3B). Although H4K20 methylation enrichments were ~2 or 3× lower compared to iDSBs, 53BP1 occupancy relative to H4K20 methylation was similar to iDSBs (Figures 2B and 3A). In contrast, H4K20 methylations and 53BP1 occupancy were not observed following PR-Set7 CD localization. The collective results demonstrate that PR-Set7 recruitment to an iDSB or an undamaged locus is necessary and sufficient to induce de novo H4K20 methylations and 53BP1 nucleation in a PR-Set7 monomethyltransferase-dependent manner.

Suv4-20 Methyltransferases Are Required for H4K20me2 and 53BP1 Nucleation at an iDSB

Based on the findings above, we hypothesized that PR-Set7-mediated H4K20me1 near DSBs facilitates subsequent

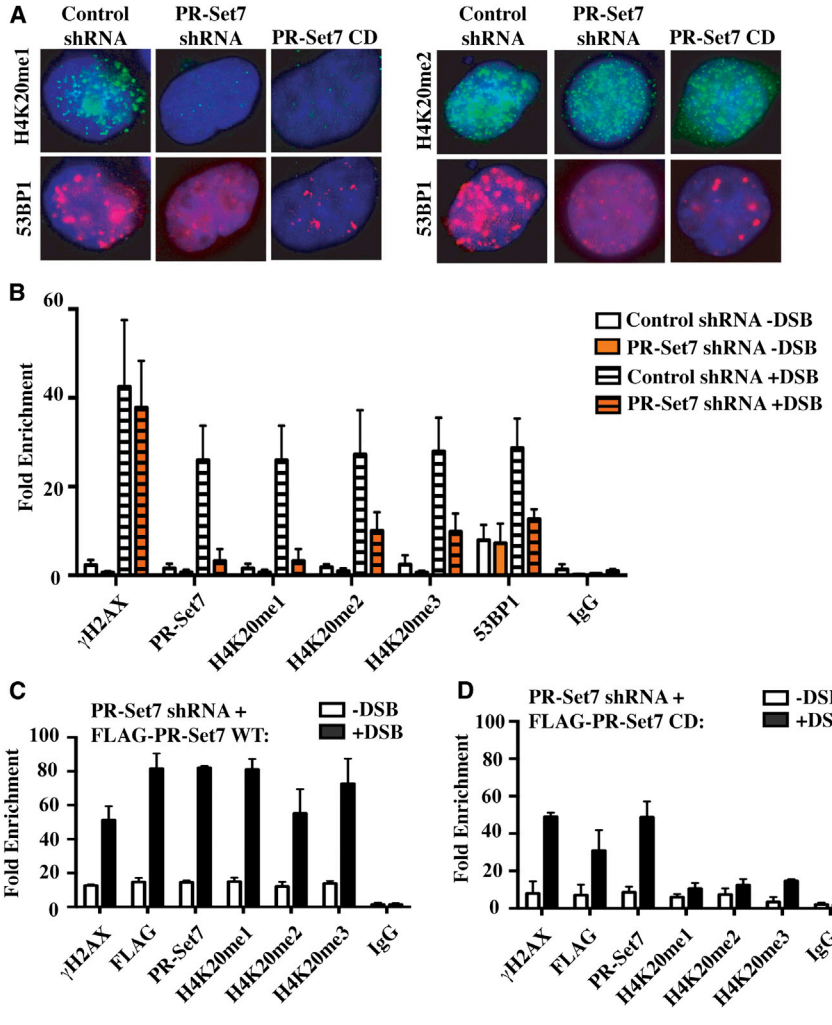

Figure 2. 53BP1 Recruitment Requires PR-Set7 Monomethyltransferase-Dependent De Novo H4K20 Methylations

(A) Representative immunofluorescence microscopy images of H4K20me1, H4K20me2 (green), and 53BP1 (red) in irradiated HeLa cells expressing control shRNA, PR-Set7-specific shRNA, or a PR-Set7 catalytically dead (CD) mutant. Cells were counterstained with DAPI (blue).

(B) ChIP-qPCR analysis near the iDSB (−1 kb) in U2OS *DR-GFP* cells transduced with control or PR-Set7 shRNA in the absence (−DSB) or presence (+DSB) of *I-SceI* using the indicated antibodies (*x* axis). Values represent the mean fold enrichment relative to histone H3 ± SD from five independent biological replicates.

(C and D) ChIP-qPCR analysis in PR-Set7-depleted U2OS *DR-GFP* cells complemented with FLAG-PR-Set7 WT (C) or FLAG-PR-Set7 CD (D) as described in Figure 2B. Values represent the mean fold enrichment relative to histone H3 ± SD from five independent biological replicates.

See also Figure S2.

H4K20me2 by a different methyltransferase. It was previously reported that the MMSET/NSD2/WHSC1 methyltransferase was required for H4K20me2 and 53BP1 recruitment (Hajdu et al., 2011; Pei et al., 2011). However, our results and recent independent reports demonstrate that MMSET does not regulate H4K20 methylation, MMSET is not recruited to DSBs, and MMSET is dispensable for 53BP1 IRIF (Figures S4G–S4L) (Hartlerode et al., 2012; Hsiao and Mizzen, 2013; Kuo et al., 2011).

In contrast to MMSET, the Suv4-20h1 and Suv4-20h2 methyltransferases are responsible for the majority of H4K20me2 and H4K20me3 in mammalian cells and H4K20me1 is the preferred substrate for Suv4-20 catalysis (Schotta et al., 2004, 2008; Southall et al., 2014; Wu et al., 2013). To test the hypothesis that the Suv4-20s are required for H4K20me2 and 53BP1 nucleation at an iDSB, the *DR-GFP* transgene was inserted at the *hprt* locus in Suv4-20h1/Suv4-20h2 double-knockout (DKO) mESCs (Donoho et al., 1998; Schotta et al., 2008). The DKO *DR-GFP* mESCs displayed similar levels of γH2A.X enrichment near the iDSB as control (Figures 1D, 3B, and S3C). Consistent with the hypothesis, significantly reduced H4K20me2, H4K20me3, and 53BP1 occupancy, but increased H4K20me1, were observed near the iDSB in the DKO *DR-GFP* mESCs compared to control. These results indicate that Suv4-20h1 and/or Suv4-20h2 are required for de novo H4K20me2 and 53BP1 nucleation near an iDSB, consistent with reports demonstrating impaired 53BP1 IRIF in Suv4-20-depleted human cells (Hsiao and Mizzen, 2013; Yang et al., 2008). The findings also demonstrate that the Suv4-20s are dispensable for PR-Set7 recruitment to DSBs; that PR-Set7 specifically monomethylates H4K20 near DSBs; and that, although 53BP1 binds H4K20me1 in vitro, PR-Set7-mediated H4K20me1 is insufficient for 53BP1 nucleation in cells (Botuyan et al., 2006; Oda et al., 2010).

PR-Set7-Mediated H4K20me1 Is Requisite for Suv4-20 Catalysis and 53BP1 Nucleation

We hypothesized that Suv4-20-dependent H4K20me2 and 53BP1 nucleation near DSBs required prior PR-Set7-mediated H4K20me1. To address this first, control or PR-Set7-depleted U2OS *DR-GFP* cells were transfected with FLAG-Suv4-20H1 or -Suv4-20H2 (Figure S3D). ChIP-qPCR analysis demonstrated equivalent enrichment of each Suv4-20, indicating that both are recruited to the iDSB in control cells (Figures 3C and S3E). PR-Set7 depletion resulted in an ~2 or 3× reduction in Suv4-20 occupancy near the iDSB, indicating that Suv4-20 recruitment is dependent, in part, on PR-Set7 and/or H4K20me1 (Figures 3C and S3F). To evaluate the necessity of H4K20me1 for Suv4-20 catalysis and 53BP1 nucleation, HEK293-TK22 cells were transfected with GAL4-DBD-Suv4-20H1 or -Suv4-20H2 (Figure S3A). In contrast to PR-Set7 WT,

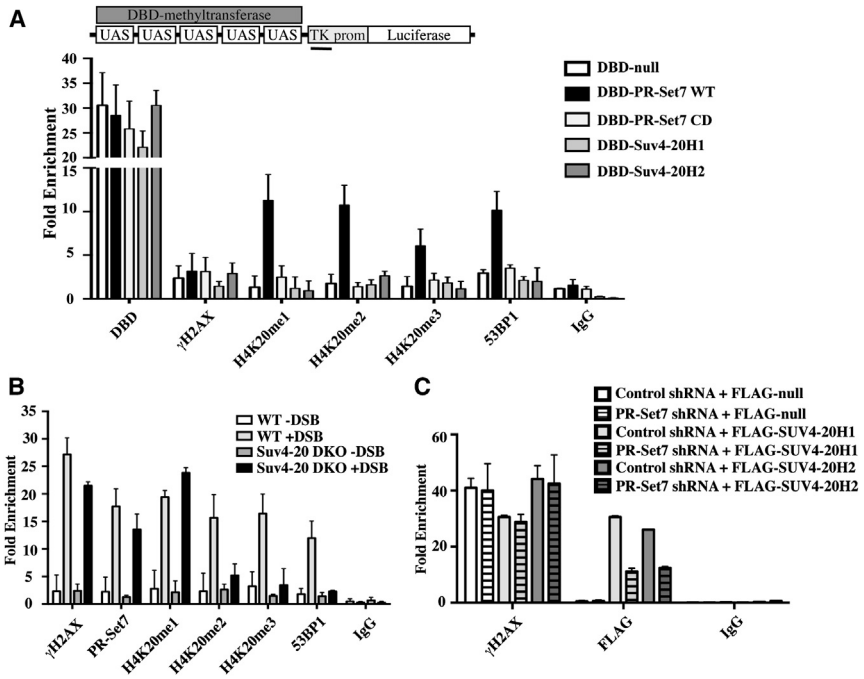

Figure 3. 53BP1 Nucleation Requires H4K20me1-Dependent Suv4-20 Recruitment and Catalysis at DSBs

(A) Illustration of the integrated *5xGAL4-UAS-TK-Luc* transgene in HEK293-TK22 cells and location of qPCR amplicon. ChIP-qPCR analysis from cells transfected with GAL4-DBD-null, -PR-Set7 WT, -PR-Set7 CD, -Suv4-20H1, or -Suv4-20H2 using the indicated antibodies (*x* axis). Values represent the mean fold enrichment relative to histone H3 ± SD from three independent biological replicates.

(B) ChIP-qPCR analysis near the iDSB (−1 kb) in WT *DR-GFP* mESCs and *Suv4-20h1/Suv4-20h2* double-knockout (DKO) *DR-GFP* mESCs as described in Figure 1D. Values represent the mean fold enrichment relative to histone H3 ± SD from three independent biological replicates.

(C) ChIP-qPCR analysis near the iDSB (−1 kb) in control or PR-Set7 shRNA U2OS *DR-GFP* cells expressing FLAG-null, -Suv4-20H1, or -Suv4-20H2 as described in Figure 2B. Values represent the mean fold enrichment relative to histone H3 ± SD from three independent biological replicates.

See also Figure S3.

ChIP-qPCR analysis demonstrated that Suv4-20 localization to the undamaged integrated transgene was insufficient for de novo H4K20 methylation and 53BP1 nucleation (Figures 3A and S3B). These findings demonstrate that PR-Set7-mediated H4K20me1 is required for proficient Suv4-20 recruitment and catalysis to generate de novo H4K20me2 near DSBs necessary for 53BP1 nucleation.

Proficient Recruitment of PR-Set7 to DSBs Is Dependent on Ku70

A previous report demonstrated that cytological accumulation of ectopic PR-Set7 at laser-induced DSB foci required direct binding to PCNA (Oda et al., 2010). To determine the necessity of PCNA binding on PR-Set7 recruitment to an iDSB, PR-Set7-depleted U2OS *DR-GFP* cells were transfected with FLAG-PR-Set7 WT or -PR-Set7 PIPm2, which encodes mutations in the second PCNA-interacting protein (PIP) box of PR-Set7 that ablates PCNA binding (Figure S4B) (Abbas et al., 2010; Centore et al., 2010; Jørgensen et al., 2011). Despite the inability to bind PCNA, ChIP-qPCR analysis revealed significant enrichments of PR-Set7 PIPm2 and H4K20 methylations near the iDSB, although these values were proportionally lower compared to PR-Set7 WT (Figures 4A and S4A). These results demonstrate that PR-Set7 recruitment to an iDSB can occur independent of PCNA binding.

To identify potential PR-Set7-interacting proteins necessary for PR-Set7 recruitment to DSBs, two independent tandem affinity purifications of ectopically expressed FLAG-hemagglutinin-null and -PR-Set7 in HeLa cells were performed followed by comparative mass spectrometry analyses (Spektor and Rice, 2009). Identification of proteins unique to PR-Set7 included the NHEJ-associated factors Ku70, Ku80, and PARP1 (Table S1). Immunoprecipitation of FLAG-PR-Set7 or -GFP negative control expressed in HEK293 cells confirmed the specific interaction of PR-Set7 with endogenous Ku70, Ku80, and PARP1 (Figure 4B). In vitro assays demonstrated that recombinant PR-Set7 directly binds Ku70 and Ku80, but not PARP1 (Figure 4C).

These findings suggested that PR-Set7 recruitment to DSBs is dependent on certain NHEJ-associated factors. To determine the necessity of specific canonical NHEJ factors on PR-Set7 recruitment to an iDSB, ChIP-qPCR was performed in several *DR-GFP* mESC lines lacking individual NHEJ factors. In *Ku70*$^{-/-}$ *DR-GFP* mESCs, PR-Set7 recruitment and de novo H4K20 methylations near the iDSB were severely impaired compared to WT control (Figures 1D, 4E, and S4C). Consistent with this, GFP-PR-Set7 mobilization to laser-induced DSBs was blunted in Ku70-depleted HeLa cells (Figure 4D). These results demonstrate that proficient PR-Set7 recruitment to DSBs is dependent on Ku70; however, PR-Set7 was found to be dispensable for Ku70 localization to DSBs (Figures S4F and S4G). In *DNA-PKcs*$^{-/-}$ *DR-GFP* mESCs, PR-Set7 recruitment and de novo H4K20 methylations near the iDSB were lower compared to WT control (Figures 1D, 4F, and S4D). These results suggest that proficient PR-Set7 recruitment to DSBs requires DNA-PKcs, consistent with the interaction detected between PR-Set7 and endogenous DNA-PKcs in HEK293 cells (Figure 4B). However, the concurrent reduction of Ku70 near the iDSB in these cells alternatively suggests that the observed decreased PR-Set7 occupancy was Ku70-dependent. In *XRCC4*$^{-/-}$ *DR-GFP* mESCs, PR-Set7 and H4K20 methylations near the iDSB were comparable to WT control, indicating that XRCC is dispensable for PR-Set7 recruitment (Figures 1D, 4G, and S4E). These collective results demonstrate that proficient PR-Set7 recruitment to DSBs is dependent on Ku70.

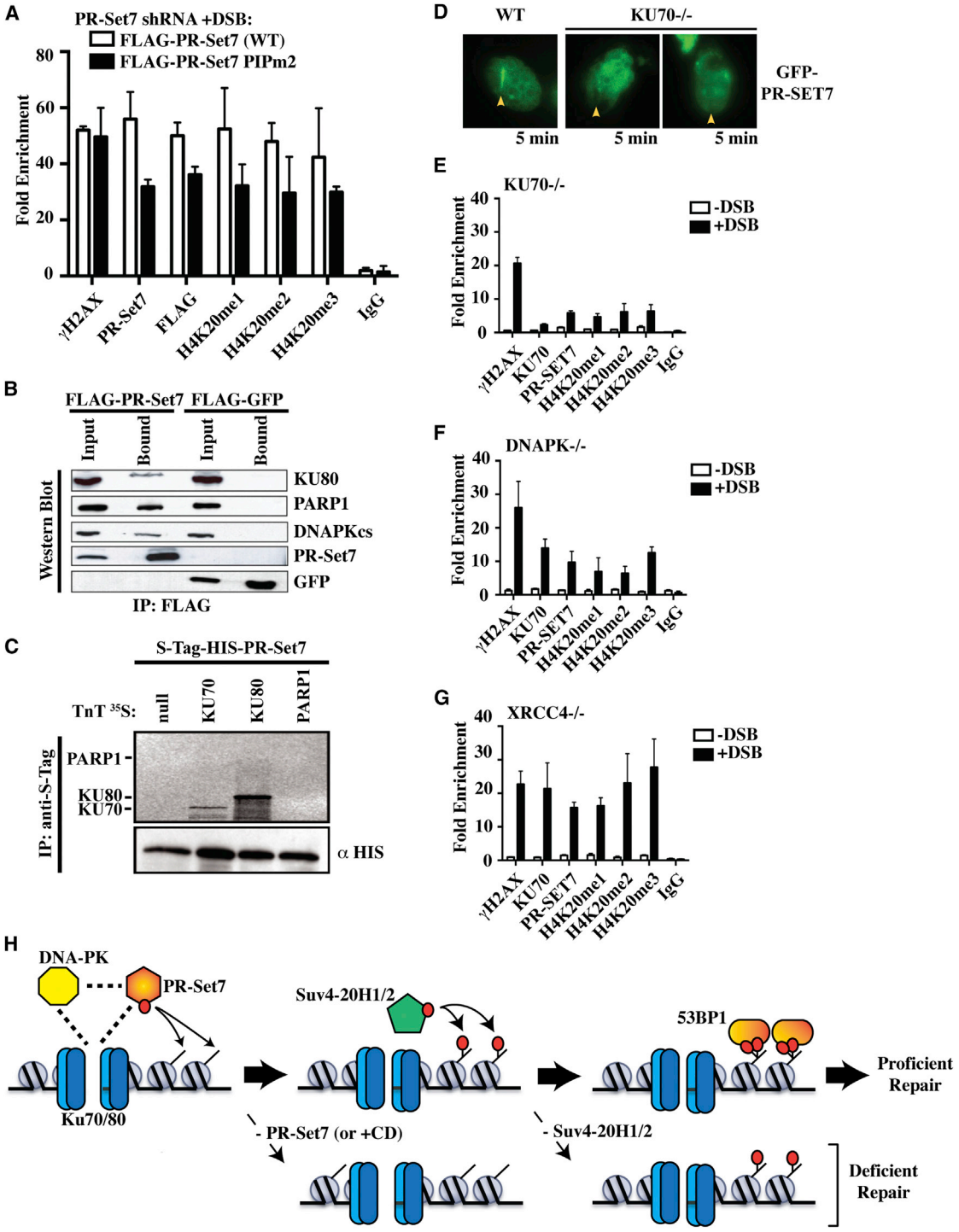

Figure 4. Ku70-Dependent Recruitment of PR-Set7 to DSBs

(A) ChIP-qPCR analysis near the iDSB (−1 kb) in control and PR-Set7 shRNA U2OS *DR-GFP* cells expressing FLAG-PR-Set7 WT or -PR-Set7 PIPm2. Values represent the mean fold enrichment relative to histone H3 ± SD from three independent biological replicates.

(B) FLAG-immunoprecipitations from nuclear lysates of HEK293 cells expressing FLAG-PR-Set7 or -GFP negative control followed by western blot analysis using the indicated antibodies. Five percent of the input material and 20% of the bound material was used. IP, immunoprecipitation.

(C) Autoradiography of SDS-PAGE-fractionated proteins following S-Tag-immunoprecipitation of recombinant S-Tag-HIS-PR-Set7 incubated with in vitro transcribed and translated (TnT) ^{35}S null, -Ku70, -Ku80, or -PARP1 (top). Equivalent immunoprecipitation between samples was assessed by western blot analysis for HIS (bottom).

(legend continued on next page)

DISCUSSION

This study reveals that recruitment of PR-Set7 to DSBs is required to induce de novo H4K20 methylation, 53BP1 nucleation, and NHEJ-directed repair (Figure 4H). PR-Set7 recruitment to laser-induced DSBs was previously reported to require direct binding of PR-Set7 to PCNA (Oda et al., 2010). The observed accumulation and retention of PR-Set7 at laser-induced DSBs, however, was inconsistent with reports demonstrating that PCNA binding results in the rapid degradation of PR-Set7 (Abbas et al., 2010; Centore et al., 2010; Jørgensen et al., 2011; Oda et al., 2010). Our results demonstrate that loss of PCNA binding had little effect on PR-Set7 recruitment to an iDSB and, alternatively, that proficient PR-Set7 recruitment to iDSBs and laser-induced DSBs was dependent on the canonical NHEJ Ku70 protein, suggesting a role for PR-Set7 in NHEJ. Consistent with this, NHEJ-directed repair was severely impaired in PR-Set7-depleted cells concurrent with the accumulation of unrepaired DSBs (Houston et al., 2008; Oda et al., 2009). These results identify PR-Set7 as an essential component of NHEJ-directed repair necessary for the maintenance of genomic stability.

Based on our findings and previous reports, we propose that PR-Set7 is a primary early determinant of DSB repair pathway choice that promotes NHEJ-directed repair. The observed rapid recruitment of PR-Set7 to DSBs and the PR-Set7-dependent de novo H4K20me2 required for subsequent 53BP1 localization to DSBs supports an early direct mechanism for PR-Set7 in promoting NHEJ-directed repair (Oda et al., 2010). This is further supported by the findings that PR-Set7 recruitment to an undamaged locus induced de novo H4K20me2 and 53BP1 nucleation, implicating PR-Set7 as a principal initiating factor of NHEJ-directed repair. It was previously reported that PR-Set7 protein levels are dynamically regulated during cell cycle progression where PR-Set7 is abundant in G1-phase, when NHEJ is the dominant DSB repair pathway, but depleted in S phase, when HDR dominates (Wu et al., 2010). These findings suggest that the regulation of PR-Set7 abundance is a central determinant of DSB repair pathway choice where the presence of PR-Set7 directly promotes NHEJ-directed repair and absence of PR-Set7 indirectly promotes HDR by impeding NHEJ-directed repair. Consistent with this, PR-Set7 depletion severely impaired NHEJ-directed repair and, concurrently, significantly enhanced HDR. The necessity for PR-Set7 degradation during initiation of fundamental HDR-associated programs, including DNA replication and UV damage repair, further supports the model that PR-Set7 regulates DSB repair pathway choice (Abbas et al., 2010; Centore et al., 2010; Jørgensen et al., 2011).

PR-Set7 monomethyltransferase activity was found to be necessary, but insufficient, for de novo H4K20me2 and 53BP1 nucleation. We determined that PR-Set7-mediated H4K20me1 functions to facilitate subsequent Suv4-20 recruitment and catalysis required to generate H4K20me2 and nucleate 53BP1 at an iDSB and an undamaged locus. Previous reports suggested that Suv4-20 and H4K20me2 were dispensable, but that H4K20me1 was sufficient, for 53BP1 recruitment because 53BP1 also binds H4K20me1 in vitro and *Suv4-20* DKO primary mouse embryonic fibroblasts (pMEFs), which have reduced global H4K20me2 but elevated H4K20me1, displayed only minor 53BP1 IRIF defects (Botuyan et al., 2006; Hartlerode et al., 2012; Oda et al., 2010; Schotta et al., 2008). In contrast to DKO pMEFs, Suv4-20-depleted HeLa cells, which also have reduced global H4K20me2 and elevated H4K20me1, displayed significant 53BP1 IRIF defects (Hsiao and Mizzen, 2013; Yang et al., 2008). Whereas the reasons for these differences remain unclear, a report demonstrating that *Suv4-20* DKO B cells displayed significantly impaired CSR supports the necessity of Suv4-20 and H4K20me2 for 53BP1 localization and function (Bothmer et al., 2011; Schotta et al., 2008). Consistent with these reports, our results directly demonstrate that PR-Set7-mediated H4K20me1 alone is insufficient, and that Suv4-20-mediated H4K20me2 is required, for 53BP1 nucleation at an iDSB. The collective results of this study indicate that the orchestrated and concerted activities of PR-Set7 and Suv4-20 are requisite rate-limiting steps for proficient 53BP1 localization and NHEJ-directed repair. Because H4K20me2-dependent binding of 53BP1 to chromatin is augmented by additional histone modifications, including H4K16 deacetylation and H2AK15 ubiquitination, we propose that the de novo generation of a DSB-specific "histone code" facilitates the selective recruitment and retention of 53BP1 at DSBs necessary for proficient NHEJ-directed repair (Fradet-Turcotte et al., 2013; Hsiao and Mizzen, 2013; Tang et al., 2013).

EXPERIMENTAL PROCEDURES

U2OS, HFF, HEK293, mESCs, and HeLa cells were cultured as previously described (Houston et al., 2008; Sims and Rice, 2008). Glycofect (Techulon) was used to transfect U2OS, and Lipofectamine 2000 (Invitrogen) was used to transfect HEK293 and HeLa according to manufacturer's instructions. The mESCs were electroporated as previously described (Donoho et al., 1998). Lentivirus was produced and cells transduced as previously reported (Sims and Rice, 2008). Approximately 10^6 U2OS or 5×10^6 mESC *DR-GFP* cells were used for each ChIP as previously described (Congdon et al., 2010). ChIPs were performed 24 or 36 hr following *I-SceI* transfection in U2OS or mESC *DR-GFP* cells, respectively, when γH2A.X enrichment was determined to be maximal at the iDSB. Other ChIP antibodies used in the studies were first

(D) Representative fluorescence microscopy images of WT or Ku70-depleted HeLa cells expressing GFP-PR-Set7 (green) 5 min after generation of laser-induced DSBs (yellow arrows).
(E–G) ChIP-qPCR analysis near the iDSB (−1 kb) in *Ku70*$^{-/-}$ (E), *DNA-PKcs*$^{-/-}$ (F), or *XRCC4*$^{-/-}$ (G) *DR-GFP* mESCs in the presence (+DSB) or absence (−DSB) of *I-SceI* using the indicated antibodies (*x* axis). Values represent the mean fold enrichment relative to histone H3 ± SD from five independent biological replicates.
(H) Proposed model. PR-Set7 interaction with canonical NHEJ factors, including Ku70/Ku80 and DNA-PKcs, results in rapid recruitment of PR-Set7 and de novo H4K20me1 at DSBs (first panel). PR-Set7-mediated H4K20me1 is required for subsequent Suv4-20 recruitment and catalysis to generate H4K20me2 at the lesion (second panel). The orchestrated recruitment and concerted enzymatic activities of PR-Set7 and Suv4-20 are necessary for 53BP1 nucleation at the DSB and NHEJ-directed repair (third panel).
See also Figure S4.

Please cite this article in press as: Tuzon et al., Concerted Activities of Distinct H4K20 Methyltransferases at DNA Double-Strand Breaks Regulate 53BP1 Nucleation and NHEJ-Directed Repair, Cell Reports (2014), http://dx.doi.org/10.1016/j.celrep.2014.06.013

titrated at these time points to optimize enrichment levels near the iDSB in control cells and compensate for possible differences in avidity between different antibodies. An iQ5 iCycler (Bio-Rad) was used for qPCR with data presented as fold enrichment (%IP/%Input)/(%IP H3/%Input H3) and statistical significance determined by the Student's t test. Western blot analysis, immunoprecipitations, comparative mass spectrometry analysis, and in vitro binding assays were performed as previously described (Spektor and Rice, 2009). Laser irradiation and immunofluorescence studies were performed as previously reported (Kong et al., 2009; Wu et al., 2010). Detailed descriptions of the reagents and methods used can be found in Supplemental Information.

SUPPLEMENTAL INFORMATION

Supplemental Information includes Supplemental Experimental Procedures, four figures, and one table and can be found with this article at http://dx.doi.org/10.1016/j.celrep.2014.06.013.

ACKNOWLEDGMENTS

This project was supported by the NIH (GM075094 to J.C.R.; CA100710 to K.Y.), an NIH Training Grant (5T32CA009320 to C.T.T.), an NCI Cancer Center Support Grant (P30CA014089), the American Cancer Society (RSG117619 to J.C.R.; PF0627301 to C.T.T.), the Margaret E. Early Research and Pew Charitable Trusts (to J.C.R.), and Deutsche Forschungsgemeinschaft (SFB1064, SFB684, and SPP1356 to G.S.). We thank Danny Reinberg (NYU, HHMI) for PR-Set7 plasmids, Mitch Lazar (UPenn) for HEK293-TK22 cells, Maria Jasin (MSKCC) for *DR-GFP* mESCs, and Jeremy Stark (City of Hope) for U2OS *DR-GFP* cells and insightful discussions.

Received: May 12, 2014
Revised: June 4, 2014
Accepted: June 9, 2014
Published: July 3, 2014

REFERENCES

Abbas, T., Shibata, E., Park, J., Jha, S., Karnani, N., and Dutta, A. (2010). CRL4(Cdt2) regulates cell proliferation and histone gene expression by targeting PR-Set7/Set8 for degradation. Mol. Cell *40*, 9–21.

Bennardo, N., Gunn, A., Cheng, A., Hasty, P., and Stark, J.M. (2009). Limiting the persistence of a chromosome break diminishes its mutagenic potential. PLoS Genet. *5*, e1000683.

Bothmer, A., Robbiani, D.F., Di Virgilio, M., Bunting, S.F., Klein, I.A., Feldhahn, N., Barlow, J., Chen, H.T., Bosque, D., Callen, E., et al. (2011). Regulation of DNA end joining, resection, and immunoglobulin class switch recombination by 53BP1. Mol. Cell *42*, 319–329.

Botuyan, M.V., Lee, J., Ward, I.M., Kim, J.E., Thompson, J.R., Chen, J., and Mer, G. (2006). Structural basis for the methylation state-specific recognition of histone H4-K20 by 53BP1 and Crb2 in DNA repair. Cell *127*, 1361–1373.

Bunting, S.F., Callén, E., Wong, N., Chen, H.T., Polato, F., Gunn, A., Bothmer, A., Feldhahn, N., Fernandez-Capetillo, O., Cao, L., et al. (2010). 53BP1 inhibits homologous recombination in Brca1-deficient cells by blocking resection of DNA breaks. Cell *141*, 243–254.

Centore, R.C., Havens, C.G., Manning, A.L., Li, J.M., Flynn, R.L., Tse, A., Jin, J., Dyson, N.J., Walter, J.C., and Zou, L. (2010). CRL4(Cdt2)-mediated destruction of the histone methyltransferase Set8 prevents premature chromatin compaction in S phase. Mol. Cell *40*, 22–33.

Congdon, L.M., Houston, S.I., Veerappan, C.S., Spektor, T.M., and Rice, J.C. (2010). PR-Set7-mediated monomethylation of histone H4 lysine 20 at specific genomic regions induces transcriptional repression. J. Cell. Biochem. *110*, 609–619.

Donoho, G., Jasin, M., and Berg, P. (1998). Analysis of gene targeting and intrachromosomal homologous recombination stimulated by genomic double-strand breaks in mouse embryonic stem cells. Mol. Cell. Biol. *18*, 4070–4078.

Fradet-Turcotte, A., Canny, M.D., Escribano-Díaz, C., Orthwein, A., Leung, C.C., Huang, H., Landry, M.C., Kitevski-LeBlanc, J., Noordermeer, S.M., Sicheri, F., and Durocher, D. (2013). 53BP1 is a reader of the DNA-damage-induced H2A Lys 15 ubiquitin mark. Nature *499*, 50–54.

Gunn, A., and Stark, J.M. (2012). I-SceI-based assays to examine distinct repair outcomes of mammalian chromosomal double strand breaks. Methods Mol. Biol. *920*, 379–391.

Hajdu, I., Ciccia, A., Lewis, S.M., and Elledge, S.J. (2011). Wolf-Hirschhorn syndrome candidate 1 is involved in the cellular response to DNA damage. Proc. Natl. Acad. Sci. USA *108*, 13130–13134.

Hartlerode, A.J., Guan, Y., Rajendran, A., Ura, K., Schotta, G., Xie, A., Shah, J.V., and Scully, R. (2012). Impact of histone H4 lysine 20 methylation on 53BP1 responses to chromosomal double strand breaks. PLoS ONE *7*, e49211.

Houston, S.I., McManus, K.J., Adams, M.M., Sims, J.K., Carpenter, P.B., Hendzel, M.J., and Rice, J.C. (2008). Catalytic function of the PR-Set7 histone H4 lysine 20 monomethyltransferase is essential for mitotic entry and genomic stability. J. Biol. Chem. *283*, 19478–19488.

Hsiao, K.Y., and Mizzen, C.A. (2013). Histone H4 deacetylation facilitates 53BP1 DNA damage signaling and double-strand break repair. J. Mol. Cell Biol. *5*, 157–165.

Ishizuka, T., and Lazar, M.A. (2003). The N-CoR/histone deacetylase 3 complex is required for repression by thyroid hormone receptor. Mol. Cell. Biol. *23*, 5122–5131.

Jørgensen, S., Eskildsen, M., Fugger, K., Hansen, L., Larsen, M.S., Kousholt, A.N., Syljuåsen, R.G., Trelle, M.B., Jensen, O.N., Helin, K., and Sørensen, C.S. (2011). SET8 is degraded via PCNA-coupled CRL4(CDT2) ubiquitylation in S phase and after UV irradiation. J. Cell Biol. *192*, 43–54.

Kong, X., Mohanty, S.K., Stephens, J., Heale, J.T., Gomez-Godinez, V., Shi, L.Z., Kim, J.S., Yokomori, K., and Berns, M.W. (2009). Comparative analysis of different laser systems to study cellular responses to DNA damage in mammalian cells. Nucleic Acids Res. *37*, e68.

Kuo, A.J., Cheung, P., Chen, K., Zee, B.M., Kioi, M., Lauring, J., Xi, Y., Park, B.H., Shi, X., Garcia, B.A., et al. (2011). NSD2 links dimethylation of histone H3 at lysine 36 to oncogenic programming. Mol. Cell *44*, 609–620.

Nishioka, K., Rice, J.C., Sarma, K., Erdjument-Bromage, H., Werner, J., Wang, Y., Chuikov, S., Valenzuela, P., Tempst, P., Steward, R., et al. (2002). PR-Set7 is a nucleosome-specific methyltransferase that modifies lysine 20 of histone H4 and is associated with silent chromatin. Mol. Cell *9*, 1201–1213.

Oda, H., Okamoto, I., Murphy, N., Chu, J., Price, S.M., Shen, M.M., Torres-Padilla, M.E., Heard, E., and Reinberg, D. (2009). Monomethylation of histone H4-lysine 20 is involved in chromosome structure and stability and is essential for mouse development. Mol. Cell. Biol. *29*, 2278–2295.

Oda, H., Hübner, M.R., Beck, D.B., Vermeulen, M., Hurwitz, J., Spector, D.L., and Reinberg, D. (2010). Regulation of the histone H4 monomethylase PR-Set7 by CRL4(Cdt2)-mediated PCNA-dependent degradation during DNA damage. Mol. Cell *40*, 364–376.

Panier, S., and Boulton, S.J. (2014). Double-strand break repair: 53BP1 comes into focus. Nat. Rev. Mol. Cell Biol. *15*, 7–18.

Pei, H., Zhang, L., Luo, K., Qin, Y., Chesi, M., Fei, F., Bergsagel, P.L., Wang, L., You, Z., and Lou, Z. (2011). MMSET regulates histone H4K20 methylation and 53BP1 accumulation at DNA damage sites. Nature *470*, 124–128.

Pesavento, J.J., Yang, H., Kelleher, N.L., and Mizzen, C.A. (2008). Certain and progressive methylation of histone H4 at lysine 20 during the cell cycle. Mol. Cell Biol. *28*, 468–486.

Sanders, S.L., Portoso, M., Mata, J., Bähler, J., Allshire, R.C., and Kouzarides, T. (2004). Methylation of histone H4 lysine 20 controls recruitment of Crb2 to sites of DNA damage. Cell *119*, 603–614.

Schotta, G., Lachner, M., Sarma, K., Ebert, A., Sengupta, R., Reuter, G., Reinberg, D., and Jenuwein, T. (2004). A silencing pathway to induce H3-K9 and H4-K20 trimethylation at constitutive heterochromatin. Genes Dev. *18*, 1251–1262.

Schotta, G., Sengupta, R., Kubicek, S., Malin, S., Kauer, M., Callén, E., Celeste, A., Pagani, M., Opravil, S., De La Rosa-Velazquez, I.A., et al. (2008). A chromatin-wide transition to H4K20 monomethylation impairs genome integrity and programmed DNA rearrangements in the mouse. Genes Dev. *22*, 2048–2061.

Sims, J.K., and Rice, J.C. (2008). PR-Set7 establishes a repressive trans-tail histone code that regulates differentiation. Mol. Cell. Biol. *28*, 4459–4468.

Southall, S.M., Cronin, N.B., and Wilson, J.R. (2014). A novel route to product specificity in the Suv4-20 family of histone H4K20 methyltransferases. Nucleic Acids Res. *42*, 661–671.

Spektor, T.M., and Rice, J.C. (2009). Identification and characterization of posttranslational modification-specific binding proteins in vivo by mammalian tethered catalysis. Proc. Natl. Acad. Sci. USA *106*, 14808–14813.

Tang, J., Cho, N.W., Cui, G., Manion, E.M., Shanbhag, N.M., Botuyan, M.V., Mer, G., and Greenberg, R.A. (2013). Acetylation limits 53BP1 association with damaged chromatin to promote homologous recombination. Nat. Struct. Mol. Biol. *20*, 317–325.

Wu, S., Wang, W., Kong, X., Congdon, L.M., Yokomori, K., Kirschner, M.W., and Rice, J.C. (2010). Dynamic regulation of the PR-Set7 histone methyltransferase is required for normal cell cycle progression. Genes Dev. *24*, 2531–2542.

Wu, H., Siarheyeva, A., Zeng, H., Lam, R., Dong, A., Wu, X.H., Li, Y., Schapira, M., Vedadi, M., and Min, J. (2013). Crystal structures of the human histone H4K20 methyltransferases SUV420H1 and SUV420H2. FEBS Lett. *587*, 3859–3868.

Yang, H., Pesavento, J.J., Starnes, T.W., Cryderman, D.E., Wallrath, L.L., Kelleher, N.L., and Mizzen, C.A. (2008). Preferential dimethylation of histone H4 lysine 20 by Suv4-20. J. Biol. Chem. *283*, 12085–12092.

SUPPLEMENTAL INFORMATION

Concerted Activities of Distinct H4K20 Methyltransferases at DNA Double Strand Breaks Regulate 53BP1 Nucleation and NHEJ-directed Repair

Creighton T. Tuzon[1], Tanya Spektor[1], Xiaodong Kong[2], Lauren M. Congdon[1], Shumin Wu[1], Gunnar Schotta[3], Kyoko Yokomori[2], and Judd C. Rice[1]

[1]University of Southern California
Keck School of Medicine
Norris Comprehensive Cancer Center
Department of Biochemistry and Molecular Biology
Los Angeles, California, USA 90033

[2]University of California at Irvine
School of Medicine
Department of Biological Chemistry
Irvine, California, USA 92697

[3]Munich Center for Integrated Protein Science
Adolf-Butenandt-Institute
Ludwig Maximilian University
Munich, 80336, Germany

SUPPLEMENTAL FIGURES

Tuzon_Figure S1

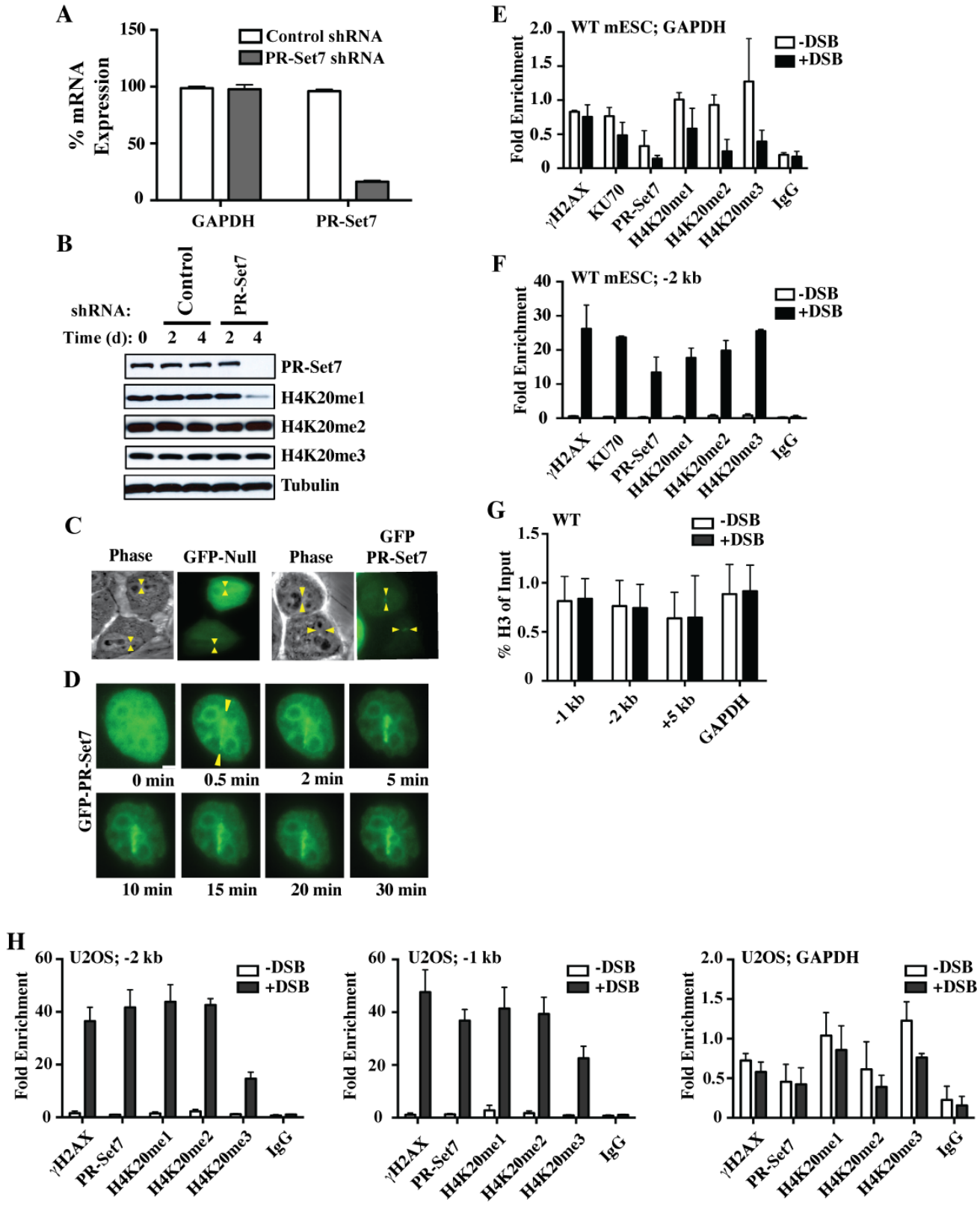

Tuzon_Figure S2

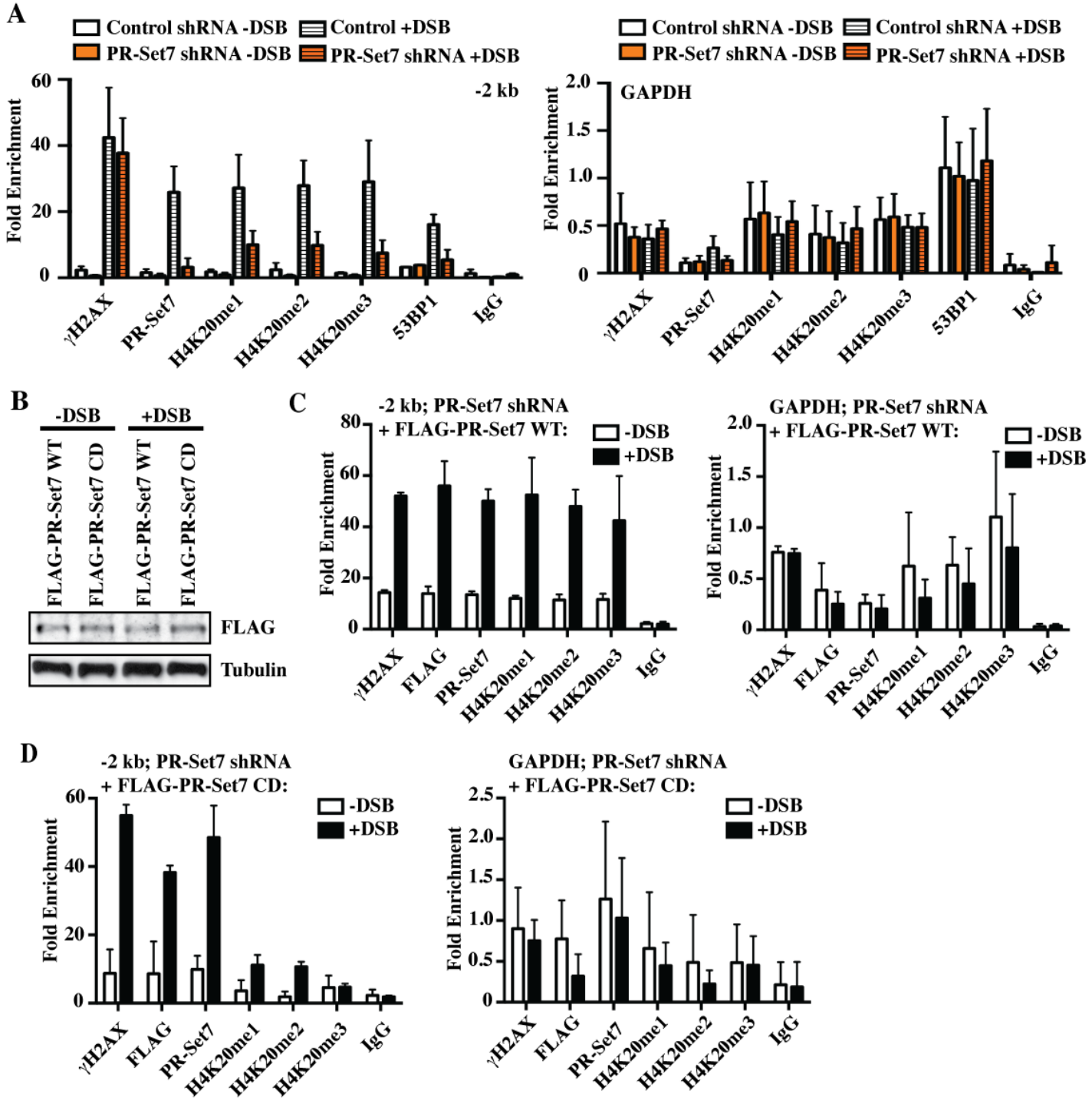

Tuzon_Figure S3

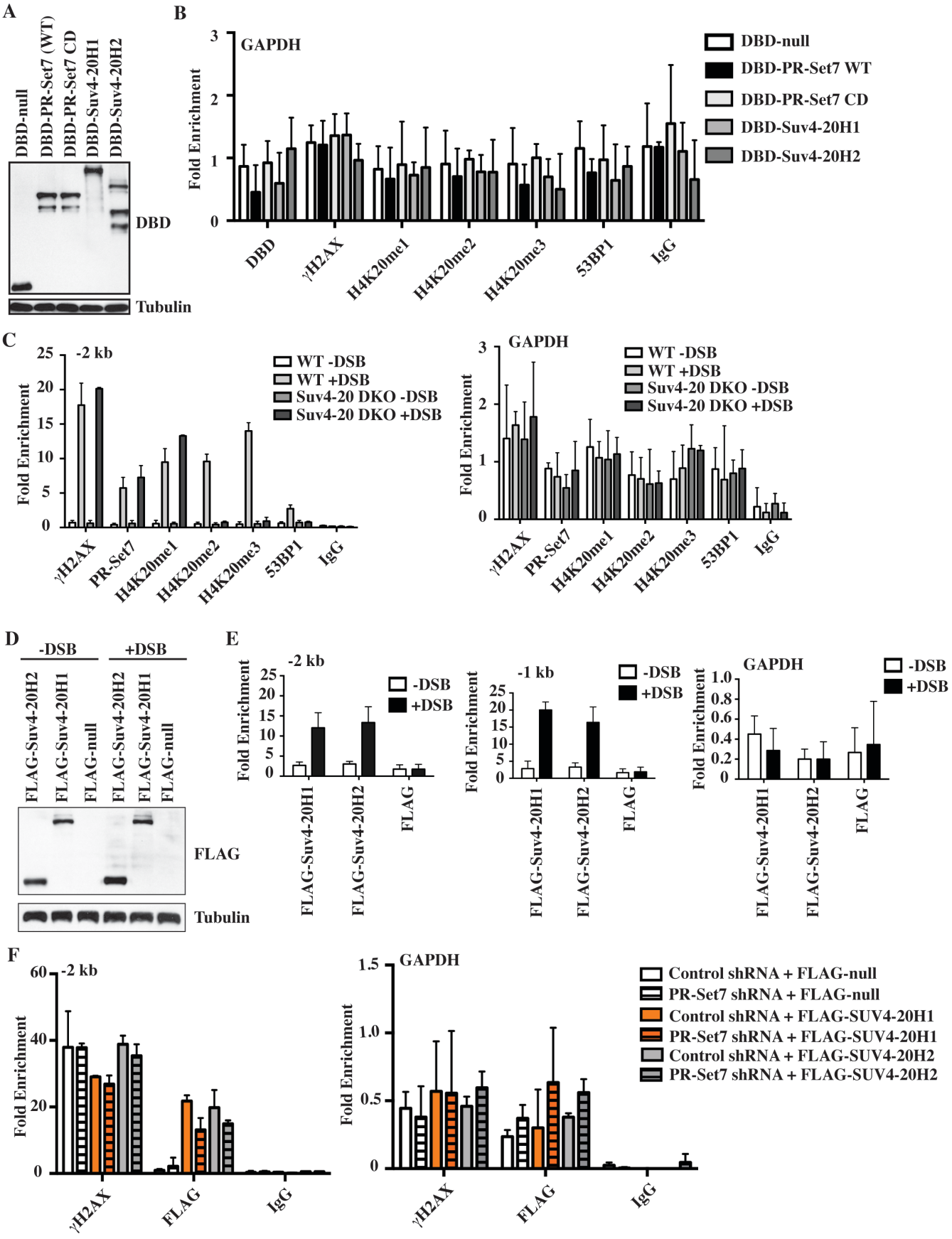

Tuzon_Figure S3

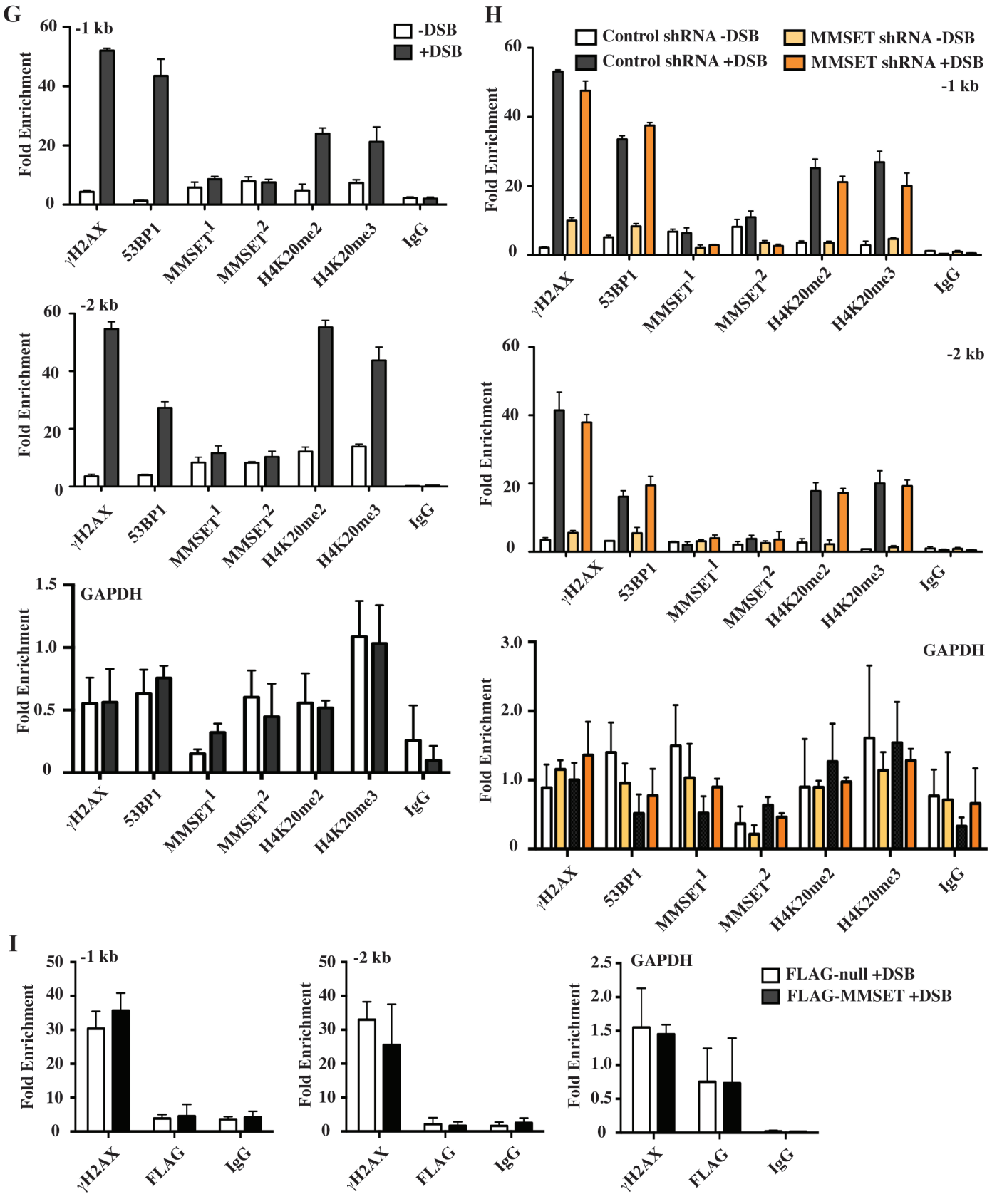

Tuzon_Figure S3

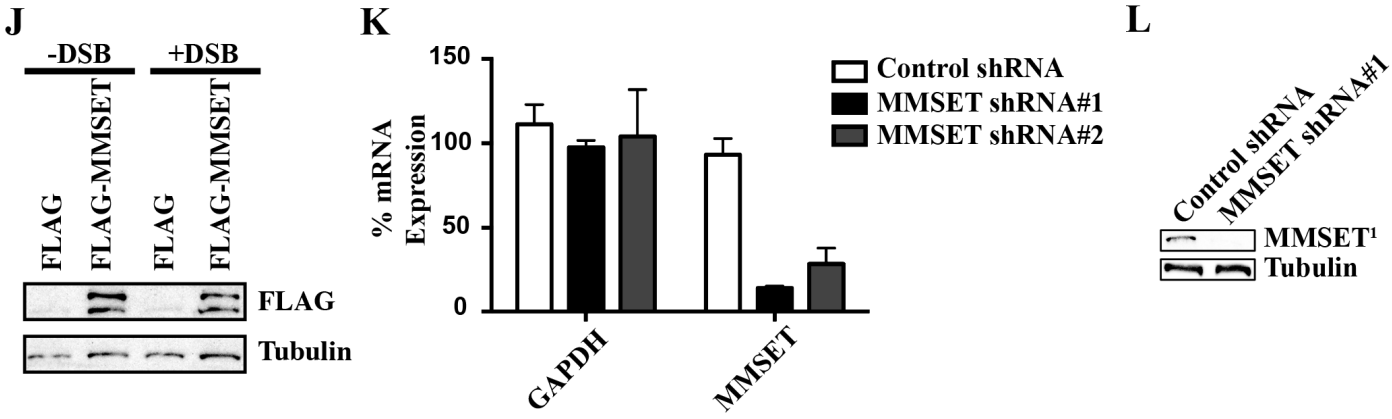

Tuzon_Figure S4

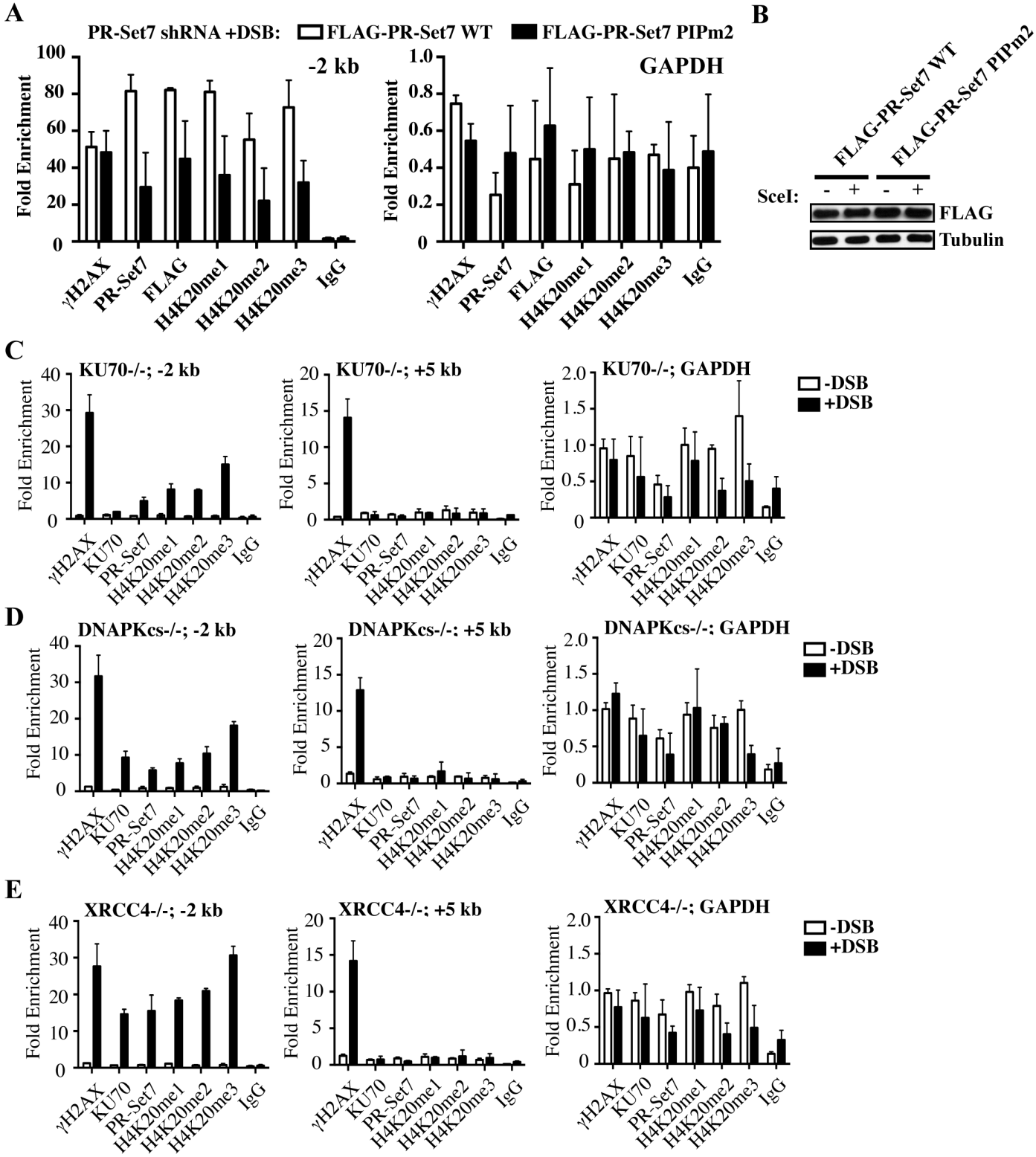

Tuzon_Figure S4

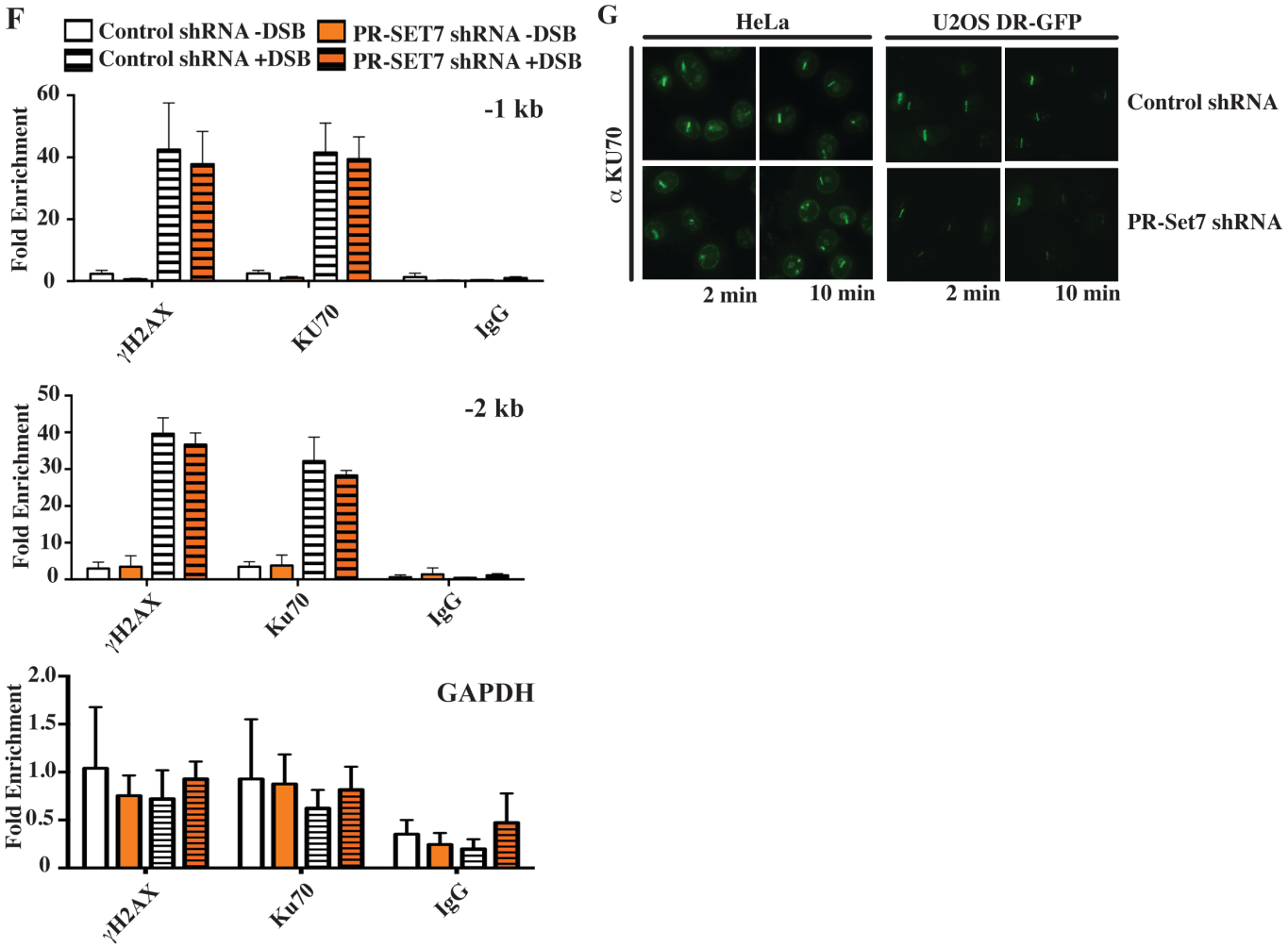

SUPPLEMENTAL FIGURE LEGENDS

Figure S1. Rapid recruitment of PR-Set7 and *de novo* H4K20 methylation near DSBs (related to Figure 1).
(A) RT-qPCR analysis of U2OS *DR-GFP* cells depleted with control and PR-Set7 shRNA. The values represent the mean +/- SD from n=5 normalized to untreated cells. (B) Representative Western blot of PR-Set7, H4K20 methylation and tubulin loading control from U2OS *DR-GFP* cells depleted with control and PR-Set7 shRNA. (C) Representative phase contrast and fluorescence microscopy images of GFP-null control or GFP-PR-Set7 HeLa cells at 10 minutes after the generation of localized DSBs by laser micro-irradiation (yellow arrows). Scale bar = 5 μm (D) Representative fluorescence microscopy time course analysis of GFP-PR-Set7 localization to laser-induced DSBs (yellow arrows). (E and F) ChIP-qPCR analysis of *DR-GFP* mESCs before (-DSB) and after (+DSB) *I-SceI* expression at (E) *GAPDH* and (F) -2 kb. The values represent the mean normalized to Histone H3 +/- SD from n=5 independent biological replicates. (G) Histone H3 ChIP-qPCR analysis of *DR-GFP* mESCs at various sites near the iDSB (x-axis). (H) ChIP-qPCR analysis of U2OS *DR-GFP* cells in the absence (-DSB) or presence (+DSB) of *I-SceI* using the indicated antibodies (x-axis) and qPCR amplicons (-1 kb, -2 kb and *GAPDH*). The values represent the mean normalized to Histone H3 +/- SD from n=5 independent biological replicates.

Figure S2. PR-Set7 is necessary for *de novo* H4K20 methylation and 53BP1 nucleation near DSBs (related to Figure 2). (A) ChIP-qPCR analysis near the iDSB (-2 kb) or at a control locus (*GAPDH*) in U2OS *DR-GFP* cells transduced with control or PR-Set7 shRNA in the absence (-DSB) or presence (+DSB) of *I-SceI* using the indicated antibodies (x-axis) as described in Figure 2B. The values represent the mean normalized to Histone H3 +/- SD from n=5 independent biological replicates. (B) Western analysis to determine FLAG-PR-Set7 WT and CD expression in Figures 2C and 2D. (C) ChIP-qPCR analysis in PR-Set7 depleted U2OS *DR-GFP* cells complemented with wild type FLAG-PR-Set7 as described in Figure 2C. Values represent the mean fold enrichment relative to Histone H3 +/- SD from n=5 independent biological replicates. (D) ChIP-qPCR analysis in PR-Set7 depleted U2OS *DR-GFP* cells complemented with catalytically dead FLAG-PR-Set7 R265G mutant (CD) as described in Figure 2D. Values represent the mean fold enrichment relative to Histone H3 +/- SD from n=5 independent biological replicates.

Figure S3. Suv4-20 methyltransferases are required, but MMSET is dispensable, for *de novo* H4K20me2, H4K20me3 and 53BP1 nucleation at DSBs (related to Figure 3). (A) Representative Western blot of DBD and tubulin loading control from ectopically expressed DBD-null, DBD-PR-Set7, DBD-PR-Set7 CD, DBD-Suv4-20H1 and DBD-Suv4-20H2 HEK293-TK22 cells. (B) ChIP-qPCR analysis at *GAPDH* negative control locus from cells transfected with GAL4-DBD-null, GAL4-DBD-PR-Set7, GAL4-DBD-PR-Set7 R265G, GAL4-DBD-Suv4-20H1 or GAL4-DBD-Suv4-20H2 using the indicated antibodies (x-axis). Values in the graph represent the mean fold enrichment normalized to Histone H3 +/- SD from n=3 independent biological replicates. (C) ChIP-qPCR analysis near the iDSB (-2 kb) and at control *GAPDH* locus in wild type mESC *DR-GFP* cells (WT) and *Suv4-20h1/Suv4-20h2* double knockout (DKO) mESC *DR-GFP* cells as described in Figure 3B. Values in the graph represent the mean fold enrichment normalized to Histone H3 +/- SD from n=3 independent biological replicates.

(D) Representative immuno-blot of ectopically expressed FLAG-null, FLAG-Suv4-20H1 and FLAG-Suv4-20H2 from U2OS *DR-GFP* in the absence (-DSB) or presence (+DSB) of *I-SceI*. (E) ChIP-qPCR analysis of ectopically expressed FLAG-null, FLAG-Suv4-20H1 and FLAG-Suv4-20H2 in U2OS *DR-GFP* cells in the absence (-DSB) or presence (+DSB) of *I-SceI* using the indicated antibodies (x-axis) and qPCR amplicons (-1 kb, -2 kb and *GAPDH*). The values represent the mean normalized to Histone H3 +/- SD from n=5 independent biological replicates. (F) ChIP-qPCR analysis near the iDSB (-2 kb) and at control *GAPDH* locus in control shRNA or PR-Set7 shRNA U2OS *DR-GFP* cells expressing FLAG-null, FLAG-Suv4-20H1 or FLAG-Suv4-20H2 in the absence (-DSB) or presence (+DSB) of *I-SceI* as described in Figure 3C. Values in the graph represent the mean fold enrichment normalized to Histone H3 +/- SD from n=3 independent biological replicates. (G) ChIP-qPCR analysis near the iDSB (-1 kb and -2 kb) transgene and at the control *GAPDH* locus in U2OS *DR-GFP* cells in the absence (-DSB) or presence (+DSB) of *I-SceI* using the indicated antibodies (x-axis). MMSET^{1} denotes the antibody used in Pei et al (Pei et al. 2011) and MMSET^{2} denotes the antibody used in Li et al (Li et al. 2009; Kuo et al. 2011). Values represent the mean fold enrichment relative to Histone H3 +/- SD from 3 independent biological replicates. (H) ChIP-qPCR analysis near the iDSB (-1 kb and -2 kb) transgene and at the control *GAPDH* locus in U2OS *DR-GFP* cells expressing control or MMSET-specific shRNA in the absence (-DSB) or presence (+DSB) of *I-SceI* using the indicated antibodies (x-axis). Values represent the mean fold enrichment relative to Histone H3 +/- SD from 4 independent biological replicates. (I) ChIP-qPCR analysis near the iDSB (-1 kb and -2 kb) transgene and at a control *GAPDH* locus in U2OS *DR-GFP* cells ectopically expressing FLAG-null control or wild type FLAG-MMSET in the presence (+DSB) of *I-SceI*. (J) Representative immuno-blot of MMSET and tubulin loading control from U2OS *DR-GFP* cells with control and MMSET shRNA#1. (K) RT-qPCR analysis of U2OS *DR-GFP* cells with control and two independent MMSET shRNAs. Values represent the mean fold enrichment relative to Histone H3 +/- SD from 4 independent biological replicates. (L) Representative immuno-blot of MMSET and tubulin loading control from U2OS *DR-GFP* cells with control and MMSET shRNA#1.

Figure S4. NHEJ Ku70-dependent recruitment of PR-Set7 to DSBs (related to Figure 4). (A) ChIP-qPCR analysis near the iDSB (-2 kb) and at control *GAPDH* locus in control shRNA and PR-Set7 shRNA U2OS *DR-GFP* cells expressing wild type FLAG-PR-Set7 (WT) or FLAG-PR-Set7 PIPm2 mutant in the presence (+DSB) of *I-SceI.* Values in the graph represent the mean fold enrichment normalized to Histone H3 +/- SD from n=3 independent biological replicates. (B) Representative immuno-blot of FLAG and tubulin loading control from PR-Set7 shRNA-depleted U2OS *DR-GFP* cells ectopically expressing wild type FLAG-PR-Set7 and FLAG-PR-Set7 PIPm2 in the absence (-DSB) and presence (+DSB) of *I-SceI*. (C-E) ChIP-qPCR analysis of *KU70-/-* (C), *DNA-PKcs-/-* (D) and *XRCC4-/-* (E) mESC *DR-GFP* cells in the absence (-DSB) or presence (+DSB) of *I-SceI* using the indicated antibodies (x-axis) and qPCR amplicons (-2 kb, +5 kb and *GAPDH*). Values in the graph represent the mean fold enrichment normalized to Histone H3 +/- SD from n=5 independent biological replicates. (F) ChIP-qPCR analysis for γH2AX, Ku70 or IgG control (x-axis) near the iDSB (-2 kb) and at the control *GAPDH* locus in control shRNA and PR-Set7 shRNA U2OS *DR-GFP* cells in the presence (+DSB) or absence (-DSB) of *I-SceI*. Values in the graph represent the mean fold enrichment normalized to Histone H3 +/- SD from n=3 independent biological replicates. (G) Representative fluorescence

microscopy images of Ku70 from control and PR-Set7 shRNA treated HeLa and U2OS *DR-GFP* cells 2 and 10 min after generation of localized DSBs by laser micro-irradiation.

Partial GO list of annotated proteins ID by Mass Spectrometry	Unique Peptides	Total Peptides
DNA Replication		
Proliferating Cell Nuclear Antigen (PCNA)	16	32
Replication Protein A, DNA Binding Subunit (RPA)	4	4
DNA Damage and Repair		
Poly ADP-Ribose Polymerase I (PARP1)	31	46
ATP-Dependent DNA Helicase II, Subunit II (KU80)	26	43
ATP-Dependent DNA Helicase II, Subunit (KU70)	12	20
RNA Processing and Splicing		
Nucleolin	19	32
Poly-Adenylate-Binding Protein I	16	18
Nucleophosmin	14	27
Heterogenous Nuclear Ribonucleoprotein Q	14	19
ATP-Dependent RNA Helicase A	14	16
Heterogeneous Nuclear Ribonucleoprotein M Isoform A	12	13
Heterogeneous Nuclear Ribonucleoprotein U	10	12
Chromatin		
Histone-Lysine N-Methyltransferase (PR-Set7)	35	313
Histone H2B	7	9
Histone H4	6	12
Histone H2A	5	5

Table S1 (related to Figure 4). Partial Gene Ontology (GO) list of PR-Set7-associated proteins identified by mass spectrometry. Nuclear extracts from FLAG-HA-PR-Set7 and FLAG-HA-null expressing HEK293 cells were used to perform tandem FLAG and HA affinity purifications as described in Supplemental Experimental Procedures. A fraction of the purified eluent was retained and fractionated by SDS-PAGE for Western analyses (Figure 4B). The remaining eluents from two independent purifications were submitted to the Taplin Mass Spectrometry Facility (Harvard University) for protein identification using the International Protein Index (IPI). Associated proteins unique to PR-Set7 or in greater abundance compared to null control with at least 4 unique peptides in the combined samples were categorized by Gene Ontology and are listed above.

SUPPLEMENTAL EXPERIMENTAL PROCEDURES

Cell culture, plasmids and transfections. U2OS, U2OS *DR-GFP*, early passage human foreskin fibroblasts (HFF), Phoenix, HEK293, HEK293-TK22, and HeLa cells were maintained at 37°C under 5% CO_2 in DMEM supplemented with 10% FBS, 1X Pen/Strep, 1X NEAA (LifeTech), and 1X L-glutamine (LifeTech). Murine *DR-GFP* embryonic stem cells were kindly provided by M. Jasin and were cultured in DMEM supplemented with 15% ES cell-qualified FBS (Millipore), 1X Pen/Strep, 1X NEAA, 1X L-glutamine, 0.1 mM 2-mercaptoethanol and 60 μl of leukemia inhibitory factor 10^7 U/ml (ESGRO). *SUV4-20* DKO mES cells were kindly provided by G. Schotta with the *DR-GFP* transgene constructed as previously described (Pierce and Jasin 2005). Plasmids pCBA and pCBA-SceI were kindly provided by M. Jasin, PR-Set7-PIPm2 by D. Reinberg, human cDNA clones of SUV4-20H1 and SUV4-20H2 by G. Schotta, along with PR-Set7 (WT) and PR-Set7-R265G were cloned into pSG5-FLAG and verified by sequencing. pLentilox3.7-null, pLentilox3.7-MMSET#1 and pLL3.7-MMSET#2 lentiviral constructs and pCAG-FLAG and pCAG-FLAG-NSD2 expression plasmids were kindly provided by O. Gozani (Kuo et al. 2011). U2OS cells were transfected with TransIT-LT1 (Mirus), U2OS *DR-GFP* cells were transfected with Glycofect (Techulon), and Phoenix and HeLa cells were transfected with Lipofectamine 2000 (LifeTech) according to manufacturer's instructions. Murine ES *DR-GFP* cells were electroporated as described previously (Weinstock et al. 2006).

shRNA, siRNA, immuno-blots and flow cytometry. Lentiviral plasmid pLKO.1 to human and murine PR-Set7 (Sigma) were co-expressed with pPAX2 and pVSV-G in Phoenix cells for lentivirus production as previously described (Sims and Rice 2008). To knockdown PR-Set7, U2OS *DR-GFP* cells were transduced twice at two-day intervals with 1:4 diluted lentiviral media prior to *SceI* induction. To verify knockdown of PR-Set7, 10% of the cell culture was used for RNA isolation in RT-qPCR analysis or for whole cell lysate immuno-blotting prior to fixation for chromatin immuno-precipitation. RT-qPCR analysis was assessed on iQ5 iCycler (Bio-Rad) using Taqman probes (Applied Biosystems) for *PR-Set7* and *GAPDH*. The two siRNAs targeting the SET domain of *MMSET* transcripts, siRNA#1: 5'-GCACACGAGAACGACATCA-3' and siRNA#2: 5'-CCACTTCTACATGCTCA-3', were applied to deplete MMSET in U2OS cells. For Western blots, protein extracts were fractionated on SDS-PAGE gels, transferred to PVDF membrane, probed with antibodies (Table 1) and detected by chemiluminescence. Chromosomal double strand break *GFP* reporters were analyzed for repair events by GFP fluorescence as previously described (Gunn and Stark 2012). Three days after transfection, live cells were typsinized, washed, resuspended in 1XPBS to 1-2X10^6 cells/ml and immediately analyzed on a LSR II (Beckton Dickson) flow cytometer acquiring 50,000 events for each GFP-based reporter.

Chromatin Immuno-Precipitation. ChIP was performed as described previously (Sims and Rice 2008; Savic et al. 2009; Pei et al. 2011; Congdon et al. 2014). Briefly, U2OS and mES *DR-GFP* cells were fixed in 1% formaldehyde for 10 min at room temperature, quenched for 5 min with 125 mM glutamine, washed extensively with PBS supplemented with 1 mM PMSF prior to lysis (50 mM Tris-HCl pH 8.1, 1% SDS, 10 mM EDTA supplemented with 1 protease inhibitor (Roche) tablet/10 ml of lysis buffer). Chromatin was sonicated for 12.5 cycles (30 sec ON and 30 sec OFF) for U2OS *DR-GFP* and 20 cycles for mES cells in a Bioruptor (Diagenode) resulting in mean chromatin length of ~500-750 bp. Approximately 1x10^6 cells for U2OS *DR-GFP* and 5x10^6 mES *DR-GFP* cells were used for each immuno-precipitation with antibodies used at an assay-dependent concentration (Table 1). In order to reproducibly achieve ChIP enrichments of

proteins and histone modifications near the iDSB, the positive control γH2AX antibody was first titrated to determine the optimal time point when γH2AX enrichment was maximal at the lowest antibody concentration following I-SceI expression: 24 hr after U2OS *DR-GFP* transfection and 36 hr after mESC *DR-GFP* electroporation (data not shown). The various antibodies used in the studies were titrated at these time points to determine enrichment levels near the iDSB comparable to γH2AX in control cells to compensate for possible differences in antibody avidity. This was especially important when antibody concentrations from serum were not known. The minimum concentrations or volumes of antibodies used for ChIPs are listed in Table 1. The negative IgG control was used at a concentration equivalent to γH2AX positive control and histone H3 positive control. Immuno-precipitated DNA was purified with ChIP DNA Clean and Concentrator (Zymo Research) kit after proteinase K and RNase A treatment. Quantitative PCR (qPCR) was analyzed on an iQ5 iCycler (Bio Rad) with the data represented as the mean fold enrichment after normalizing the percent immuno-precipitation to histone H3 [(IP/Input)/(IP of H3/Input of H3)]. PCR primer pairs used to amplify sequences adjacent to the iDSB are:
-2 Kb (Forward) 5'-GCCCATATATGGAGTTCCGC-3'
and (Reverse) 5'-CGTAAGGTCATGTACTGGGC (Niida et al. 2010);
-1 Kb (Forward) 5'-GACCGCGTTACTCCCACAGGTG-3'
and (Reverse) 5'-GGCTTTCACGCAGCCACAGAAAA;
+5 Kb (Forward) 5'-CACTAACTTGCTCACACTATCCTCG-3'
and (Reverse) 5'- TTTCTAGACCAGCCCACGTAATG;
GAPDH human (Forward) 5'-CTGGTCTAAGGAGCCTGGTG-3'
and (Reverse) 5'-GGACTGCCTATGGATCTGGA;
GAPDH murine (Forward) 5'-CAGGAGCGAGACCCCACTAA
and (Reverse) 5'-ATACTCAGCACCGGCCTCAC-3'.
Primers for qPCR from HEK293-TK22 cells were previously described (Kalakonda et al. 2008).

Irradiation, DNA Damage and Immunofluorescence (IF). U2OS cells were transduced twice at two days intervals with PR-Set7 and Control shRNA lentivirus. On day 4, cells were subjected to DNA damage by either 0-4 Gy γ-irradiation (IR) or 780nm NIR femtosecond (fs) laser microirradiation. IR was done using a Cesium-137 source irradiator. The laser micro-irradiation to generate DSBs in a defined nuclear region was performed as described previously (Kong et al. 2011). One hour after DNA damage induction by laser micro-irradiation, cells were fixed in 4% paraformaldehyde for 15 min at 4°C, permeabilized in 0.5% Triton X-100 for 5 min at 4°C, and stained with antibodies. The staining procedure was described previously (Kim et al. 2002). For cell viability measurements, U2OS cells were plated at $1x10^5$ cells. The next day, cells were transduced with either shRNA control or PR-Set7 lentivirus for 2 days, and then subjected to 2 Gy IR. Cells were cultured for an additional 2 days prior to viability analysis by trypan blue exclusion on a Cellometer Cell Counter (Nexcelcom). For HeLa IF, cells were plated on coverslips at $1x10^5$ cells/well, fixed with 2% paraformaldehyde for 10 min at RT, washed with PBS, permeabilized with 0.2% Triton X-100 for 5 min at RT, and then blocked with 5% donkey serum in PBS for 1 hr at RT. Cells were incubated with primary and secondary antibodies diluted in 5% donkey serum for 1 hr in a humidified 37°C incubator. Cells were mounted with Vectashield (Vector Lab) containing DAPI and images were captured from an inverted Zeiss Imager Z1 fluorescent microscope.

Immunoprecipitation (IP) and mass spectrometry analysis. HEK293T cells were transfected with either FLAG-HA-PR-Set7 or FLAG-HA-GFP plasmids. Approximately 36 hr after

transfection, cells were collected for nuclear extract preparation as previously described (Dignam et al. 1983). Briefly, cells were collected by low speed centrifugation, resuspended in low salt Buffer A (10 mM HEPES, pH 7.9, 1.5 mM MgCl2, 10 mM KCl, 0.5 mM DTT, 1 mM PMSF and 1 tablet Mini Complete EDTA-free protease inhibitor tablet/10 ml Buffer A (Roche)), and lysed using a dounce homogenizer with type B pestle. The crude nuclear pellet was collected by centrifugation, resuspended in Buffer C (20 mM HEPES, pH 7.9, 20% glycerol, 420 mM NaCl, 1.5 mM MgCl2, 0.2 mM EDTA, 1 mM PMSF and 1 tablet Mini Complete EDTA-free protease inhibitor tablet/10 ml Buffer C (Roche)), and then lysed by dounce homogenization with type B pestle. The nuclear protein extracts were collected from high-speed centrifugation (20,000 g), and then diluted with Buffer C without NaCl (final 150 mM). Protein concentrations were measured using the Bradford Assay (Bio-Rad) and equal protein concentrations from FLAG-HA-PR-Set7 and FLAG-HA-GFP were further diluted to reduce the glycerol concentration to 5% prior to the addition of Triton X-100 to a final concentration of 0.1%. Nuclear extracts were immune-precipitated with EZ-View Red anti-HA or anti-FLAG beads (Sigma) overnight at 4°C, and the next day washed extensively, prior to elution with 250 μg/ml FLAG peptides. The eluted proteins were concentrated by TCA precipitation and the lyophilized material was analyzed by mass spectrometry at the Taplin Mass Spectrometry Facility (Harvard University).

***In vitro* Binding Assay** Recombinant S-tag-HIS-PR-Set7 proteins were induced in BL21 *E. coli* and batch purified on Ni-Sepharose High Performance agarose beads (GE Healthcare) accordingly to the manufacturer's instructions and *in vitro* binding assays were performed as previously described (Spektor et al. 2011). Briefly, recombinant S-tag-HIS-PR-Set7 (10 μg) proteins, 2.5 μg of anti-S-tag antibody (Abcam) and 25 μL of pre-equilibrated Protein-A beads (LifeTech) in a 300 μL final volume of IP buffer (50 mM Tris-HCl, pH 7.0, 150 mM NaCl, 0.5 mM DTT, 1% NP-40, 1 mM PMSF and 1 tablet Complete Mini EDTA-free protease tablet (Roche)/10 ml buffer) were incubated overnight at 4°C. Protein extracts from in vitro translated [^{35}S]-labeled (Promega) control, KU70, KU80 and PARP1 proteins diluted in IP buffer were first pre-cleared with 25 μl Ni-Sepharose High Performance agarose beads for 2 hr at 4°C, and then extracts were added to washed pre-bound S-tag-HIS-PR-Set7-bead complex and incubated overnight at 4°C. The next day, the beads were washed extensively with IP buffer and bound proteins were eluted in SDS loading dye prior to fractionation by SDS-PAGE, Western analysis and autoradiography.

Antibodies (related to Experimental Procedures)

Antibody	ChIP	Western	Source
γH2AX	2.5 ug	1:1000	Millipore
KU70/KU80	10 ug		Thermo Fisher
KU70		1:1000	Sigma
PR-SET7	15 uL	1:1000	Abcam
H4K20me1	15 uL	1:75,000	(Sims and Rice 2008)
H4K20me1	15 uL	1:20,000	(Sims and Rice 2008)
H4K20me3	15 uL	1:5000	(Sims and Rice 2008)
53BP1	15 ug	1:1000	Novus
MMSET	10 ug	1:1000	Abcam
MMSET	10 ug	1:1000	(Li et al. 2009)
IgG	2.5 ug		Thermo Fisher
H3	2.5 ug	1:100,000	Abcam
H4		1:30,000	Abcam
α-Tubulin		1:30,000	Sigma
Flag M2	10 ug	1:1000	Sigma

SUPPLEMENTAL REFERENCES

Congdon LM, Sims JK, Tuzon CT, Rice JC. 2014. The PR-Set7 binding domain of Riz1 is required for the H4K20me1-H3K9me1 trans-tail 'histone code' and Riz1 tumor suppressor function. *Nucleic acids research*.

Dignam JD, Lebovitz RM, Roeder RG. 1983. Accurate transcription initiation by RNA polymerase II in a soluble extract from isolated mammalian nuclei. *Nucleic acids research* **11**: 1475-1489.

Gunn A, Stark JM. 2012. I-SceI-based assays to examine distinct repair outcomes of mammalian chromosomal double strand breaks. *Methods in molecular biology* **920**: 379-391.

Kalakonda N, Fischle W, Boccuni P, Gurvich N, Hoya-Arias R, Zhao X, Miyata Y, Macgrogan D, Zhang J, Sims JK et al. 2008. Histone H4 lysine 20 monomethylation promotes transcriptional repression by L3MBTL1. *Oncogene* **27**: 4293-4304.

Kim JS, Krasieva TB, LaMorte V, Taylor AM, Yokomori K. 2002. Specific recruitment of human cohesin to laser-induced DNA damage. *The Journal of biological chemistry* **277**: 45149-45153.

Kong X, Stephens J, Ball AR, Jr., Heale JT, Newkirk DA, Berns MW, Yokomori K. 2011. Condensin I recruitment to base damage-enriched DNA lesions is modulated by PARP1. *PloS one* **6**: e23548.

Kuo AJ, Cheung P, Chen K, Zee BM, Kioi M, Lauring J, Xi Y, Park BH, Shi X, Garcia BA et al. 2011. NSD2 links dimethylation of histone H3 at lysine 36 to oncogenic programming. *Mol Cell* **44**: 609-620.

Li Y, Trojer P, Xu CF, Cheung P, Kuo A, Drury WJ, 3rd, Qiao Q, Neubert TA, Xu RM, Gozani O et al. 2009. The target of the NSD family of histone lysine methyltransferases depends on the nature of the substrate. *J Biol Chem* **284**: 34283-34295.

Niida H, Katsuno Y, Sengoku M, Shimada M, Yukawa M, Ikura M, Ikura T, Kohno K, Shima H, Suzuki H et al. 2010. Essential role of Tip60-dependent recruitment of ribonucleotide reductase at DNA damage sites in DNA repair during G1 phase. *Genes Dev* **24**: 333-338.

Pei H, Zhang L, Luo K, Qin Y, Chesi M, Fei F, Bergsagel PL, Wang L, You Z, Lou Z. 2011. MMSET regulates histone H4K20 methylation and 53BP1 accumulation at DNA damage sites. *Nature* **470**: 124-128.

Pierce AJ, Jasin M. 2005. Measuring recombination proficiency in mouse embryonic stem cells. *Methods in molecular biology* **291**: 373-384.

Savic V, Yin B, Maas NL, Bredemeyer AL, Carpenter AC, Helmink BA, Yang-Iott KS, Sleckman BP, Bassing CH. 2009. Formation of dynamic gamma-H2AX domains along broken DNA strands is distinctly regulated by ATM and MDC1 and dependent upon H2AX densities in chromatin. *Molecular cell* **34**: 298-310.

Sims JK, Rice JC. 2008. PR-Set7 establishes a repressive trans-tail histone code that regulates differentiation. *Mol Cell Biol* **28**: 4459-4468.

Spektor TM, Congdon LM, Veerappan CS, Rice JC. 2011. The UBC9 E2 SUMO conjugating enzyme binds the PR-Set7 histone methyltransferase to facilitate target gene repression. *PLoS One* **6**: e22785.

Weinstock DM, Nakanishi K, Helgadottir HR, Jasin M. 2006. Assaying double-strand break repair pathway choice in mammalian cells using a targeted endonuclease or the RAG recombinase. *Methods Enzymol* **409**: 524-540.